

GCA Technical Report No. 66-8-N

CONTRIBUTIONS TO PLANETARY METEOROLOGY

George Ohring Wen Tang Frederick B. House Joseph Mariano

FINAL REPORT

Contract No. NASW-1227

March 1966

GCA CORPORATION
GCA TECHNOLOGY DIVISION
Bedford, Massachusetts

Prepared for
NATIONAL AERONAUTICS AND SPACE ADMINISTRATION
HEADQUARTERS
WASHINGTON 25, D. C.

FOREWORD

This final report is based upon research carried out during the past year on NASA contract NASW-1227, Planetary Meteorology. During the year, several investigations related to the meteorology of the planets Mars and Venus were completed and the results are presented here in the form of four separate papers. Abstracts for these four studies follow, and the papers themselves comprise Sections 1, 2, 3, and 4 of this report.

ON THE STEADY SYMMETRICAL REGIME OF THE GENERAL
CIRCULATION OF THE MARTIAN ATMOSPHERE

2100
Presented at the 1967 Proceedings

Wen Tang

ABSTRACT

21767

The model of the general circulation for steady state and symmetrical regime based upon Charney's development is modified by including the lateral eddy viscosity. The surface stress is also adjusted slightly. The resulting modified model is used to study the mean zonal and meridional winds, and the type of circulation regime on the planet Mars during the equinoctial seasons. With input parameters based on the recent occultation experiment from Mariner IV, the computed mean zonal wind at an isobaric surface of one quarter of the average surface pressure of Mars is about 36 m sec^{-1} . This compares to a value of about 33 m sec^{-1} computed for the Earth's atmosphere with the same modified model. Comparing the calculated magnitude of the atmospheric pole-to-equator temperature difference at the middle level of the atmosphere with the observed temperature difference at the same level, as deduced from the observational indications of surface temperatures, we conclude that the symmetrical regime cannot remain stable. Therefore, in the mean for the Martian year, a wave type circulation regime will prevail in the Martian atmosphere.

[Handwritten signature]

THE SEASONAL CLIMATOLOGY OF MARS

Frederick B. House

ABSTRACT

A simple theoretical model is formulated to determine the latitudinal and seasonal variation of the surface and mean atmospheric temperatures of Mars. The model assumes a single-layered, isothermal stationary atmosphere whose spectral properties are non-gray, and the temperature climate is computed from assumed conditions of radiative equilibrium.

The average annual temperature on Mars is computed for representative surface pressures and atmospheric compositions, based on recent telescopic observations and the Mariner IV radio occultation measurements. Calculations indicate a surface temperature of 215°K and a mean atmospheric temperature of 187°K . Little variation is noted in the calculated temperatures for the different pressures and compositions. Therefore, a representative atmosphere whose surface pressure is 10 mb consisting of 5 mb CO_2 , 5 mb N_2 , plus an additional 30 microns of precipitable H_2O , was selected for the seasonal climatology study.

Results indicate that the summer poles on Mars have the warmest average surface temperatures, the south pole temperature, 248°K , being somewhat warmer than the north pole temperature, 230°K . At high latitudes during the winter season, the mean atmospheric temperature is higher than the surface temperature, which suggests a strong temperature inversion at the surface. The spring and fall seasons on Mars indicate a marked similarity of the temperature climate in both hemispheres. For the annual mean, the surface and atmospheric temperatures at the equator are 226°K and 196°K , and at the poles are about 173°K and 160.5°K , respectively. The results also indicate the seasonal variation of the equatorward extension of the polar ice cap. The concluding remarks discuss the effect of the atmospheric transport of heat on the Martian temperature climate.

WATER VAPOR MIXING RATIOS NEAR THE CLOUD-TOPS OF VENUS

ICARUS

George Ohring

ABSTRACT

It has been argued that the observed amounts of water vapor in the Cytherian atmosphere are incompatible with the presence of an aqueous cloud. These arguments have been based upon a comparison of the water mixing ratios derived from the observations and the required saturation mixing ratio. In deriving the water vapor mixing ratios, it has been assumed that the water vapor mixing ratio is constant with altitude above the Cytherian cloud-top. In the present paper, it is shown that if the Cytherian water vapor mixing ratio decreases with altitude at rates comparable to those in the Earth's upper troposphere, some of the observed amounts of water vapor, at the present state of our knowledge, are compatible with the presence of aqueous clouds on Venus.

INTERHEMISPHERIC TRANSPORT OF WATER VAPOR AND THE MARTIAN ICE CAPS

George Ohring and Joseph Mariano *not*

ABSTRACT

During the course of the Martian year, as one polar ice cap forms, the other sublimates and completely disappears. The thickness of the ice cap is estimated to be of the order of 1000 times the total amount of water in the atmosphere. Thus, it has been suggested that, as one ice cap melts, the water vapor released into the atmosphere is quickly transported to the opposite pole, where it condenses. In the present study an investigation is performed to determine whether large scale atmospheric diffusion can explain such a transport and — if so — what magnitude is required for the diffusion coefficient. A diffusion model is developed in which the source of water vapor is a sublimating north polar cap that initially is one centimeter thick and extends from 60° latitude to the pole. Over a time period of $\frac{1}{2}$ Martian year this cap sublimates and the water vapor released into the atmosphere is diffused southward by a large scale eddy diffusion process with a constant diffusion coefficient. Computations with this simple model suggest that a large scale eddy diffusion coefficient of at least $10^{10} \text{ cm}^2 \text{ sec}^{-1}$ is required to accomplish the necessary interhemispheric transport of water vapor. It is also noted that a diffusion coefficient of $10^{10} \text{ cm}^2 \text{ sec}^{-1}$ leads to meridional speeds of water vapor isopleths that are in good agreement with the observed meridional speed of propagation of the Martian wave of darkening.

TABLE OF CONTENTS

<u>Section</u>	<u>Title</u>	<u>Page</u>
1	ON THE STEADY SYMMETRICAL REGIME OF THE GENERAL CIRCULATION OF THE MARTIAN ATMOSPHERE	1
2	THE SEASONAL CLIMATOLOGY OF MARS	29
3	WATER VAPOR MIXING RATIOS NEAR THE CLOUD-TOPS OF VENUS	51
4	INTERHEMISPHERIC TRANSPORT OF WATER VAPOR AND THE MARTIAN ICE CAPS	61

1. ON THE STEADY SYMMETRICAL REGIME OF THE GENERAL CIRCULATION OF THE MARTIAN ATMOSPHERE

Wen Tang

1.1 Introduction

A numerical experiment applied to the terrestrial atmospheric large scale circulation was performed first by Phillips (1956). From this model Charney (1959) modified the thermodynamic energy equation such that a column of atmosphere is heated or cooled depending upon whether its temperature is below or above its radiative temperature at the latitude in question. The present model is basically Charney's development, but the lateral eddy viscosity is included and the frictional stress acting across a horizontal surface is assumed in a slightly different form. These modifications are important to the magnitude and direction of the flow in the lower half of the atmosphere. To investigate the effect of these parameters on the computed wind velocities in the Martian atmosphere, various values of lateral eddy viscosities and coefficients of vertical eddy viscosity are used in the computations. Estimates of the most probable wind velocities on Mars are then made based upon the magnitude of the frictional parameters commonly used in general circulation models.

As a first step in the investigation of the general circulation of the Martian atmosphere, we consider here only the steady state, axially symmetric case and solve the circulation problem analytically for the two-level model.

1.2 Differential Equation and Boundary Conditions

What is usually done for the two-level model is the following: The pressure levels at $p=0$, $p_s/4$, $2p_s/4$, $3p_s/4$, and p_s are designated by the subscripts 0, 1, 2, 3, and 4 respectively, where p_s is the surface pressure. A rectangular coordinate system in the horizontal direction with x and y toward east and north respectively is used. From the equations of motion and continuity, one can obtain the quasi-geostrophic vorticity equation for levels 1 and 3 as

$$\left(\frac{\partial}{\partial t} + u_1 \frac{\partial}{\partial x} + v_1 \frac{\partial}{\partial y} \right) (\zeta_1 + \beta y) - f_0 \frac{\omega_2}{p_2} = A \nabla^2 \zeta_1 - k_i \frac{\partial}{\partial y} (u_1 - u_3) \quad (1)$$

$$\left(\frac{\partial}{\partial t} + u_3 \frac{\partial}{\partial x} + v_3 \frac{\partial}{\partial y} \right) (\zeta_3 + \beta y) + f_o \frac{\omega_2}{p_2} = A \nabla^2 \zeta_3 + k_i \frac{\partial}{\partial y} (u_1 - u_3) + K \frac{\partial}{\partial y} \left(\frac{3u_3}{2} - \frac{1}{2} u_1 \right) \quad (2)$$

where $u, v, \omega = \frac{dx}{dt}, \frac{dy}{dt}, \frac{dp}{dt}$,

ζ = the relative vorticity,

$\beta = \frac{df}{dy}$,

f_o = the mean Coriolis parameter,

$k_i = \frac{\mu g^2}{\alpha_2 p_2}$,

μ = dynamic coefficient of eddy viscosity in the vertical direction,

$\alpha_2 = \frac{\phi_1 - \phi_3}{p_2}$,

p_2 = pressure at middle of atmosphere,

∇^2 = Laplacian operator,

K = a proportional constant for the frictional stress near surface,

g = acceleration of gravity,

ϕ = geopotential,

t = time.

The quasi-geostrophic assumption in the vorticity equations is valid for the Martian atmosphere since the estimated thermal Rossby number is about 0.1 (Tang, 1965).

The first law of thermodynamics and the equation of state can be written as

$$f_o \frac{\omega_2}{p_2} = + \lambda^2 \left[\left(\frac{\partial}{\partial t} + u_2 \frac{\partial}{\partial x} + v_2 \frac{\partial}{\partial y} \right) (\psi_1 - \psi_3) - \frac{R}{c_p f_o} \frac{dQ_2}{dt} - A \frac{\partial^2}{\partial y^2} (\psi_1 - \psi_3) \right] \quad (3)$$

and

$$RT_2 \approx f_0 (\psi_1 - \psi_3) \quad (4)$$

respectively, where

$$\lambda^2 = \frac{f_0}{RT_2} \left(\frac{\theta_2}{\theta_1 - \theta_3} \right) - \text{a measure of static stability,}$$

θ = potential temperature,

$\psi = \phi/f_0$ = geostrophic stream function,

T_2 = temperature at the middle of the atmosphere,

R = gas constant for Martian atmosphere,

c_p = specific heat at constant pressure for Martian atmosphere,

$$\frac{dQ_2}{dt} = \text{radiative rate of heating per unit mass.}$$

A simple approach to compute the radiative rate of heating per unit mass, dQ_2/dt , as a function of latitude is explained below.

A prescribed heating rate as a function of latitude is not very adequate for the large scale circulation, as the atmosphere determines its own heating rate as a function primarily of its temperature distribution. In order to have such a radiative transfer mechanism tractable the following assumptions are thus made.

- (1) The atmosphere is isothermal, in the radiative sense.
- (2) The atmosphere is transparent to solar radiation.
- (3) The atmosphere is grey to long wave radiation.
- (4) The surface of the planet Mars has no heat capacity.

The total incoming solar flux for a day at a given latitude, ϕ , and solar declination, δ , is

$$Q = \frac{\tau}{\pi} S_0 \left[H_1 \sin \phi \sin \delta + \sin H_1 \cos \delta \cos \phi \right]$$

where

τ = the duration of a day (24 hrs),

S_0 = the solar constant,

and H_1 = the hour angle between sunrise and noon.

For the equinox, $\delta = 0$, $\sin H_1 = 1$, and the mean flux is

$$S = \frac{Q}{\tau} = \frac{S_o \cos \varphi}{\pi} .$$

The assumption of zero heat capacity at the ground implies that the surface is in radiative equilibrium. Therefore,

$$\frac{(1 - \epsilon) S_o \cos \varphi}{\pi} + \nu \sigma T_2^4 - \sigma T_4^4 = 0 \quad (5)$$

where ϵ = the albedo of Mars,
 ν = the absorptivity,
 σ = Stefan-Boltzmann constant.

The heating rate per unit mass of atmosphere can be written as

$$\frac{dQ_2}{dt} = \frac{1}{(2p_2)/g} [\nu \sigma T_4^4 - 2\nu \sigma T_2^4] .$$

Substituting T_4^4 from Equation (5) into the last equation yields

$$\frac{dQ_2}{dt} = \frac{g\nu(2 - \nu)\sigma}{2p_2} \left[\left(\frac{1 - \epsilon}{2 - \nu} \right) \frac{S_o \cos \varphi}{\pi \sigma} - T_2^4 \right] .$$

The first term in the bracket of the last equation corresponds to the radiative equilibrium temperature $(T_2^*)^4$ at level 2. T_2^* may be expanded into a Taylor's series near 45° latitude where $y = 0$. The first two terms of this series may be written as

$$T_2^* = \left[\left(\frac{1 - \epsilon}{2 - \nu} \right) \frac{S_o \cos \varphi}{\sigma \pi} \right]^{\frac{1}{4}} = T_R - \left(\frac{\partial T}{\partial \varphi} \frac{d\varphi}{dy} \right) y = T_R \left(1 - \frac{y}{4a} \right) \quad (6)$$

where $T_R = T_2^*(y=0)$. If the radiative equilibrium temperature, T_R , is close to the observed mean temperature at $y=0$, then we are able to linearize the heating rate per unit mass and to write

$$\begin{aligned} \frac{dQ_2}{dt} &\approx \frac{4g\nu(2 - \nu)\sigma T_m^3}{2p_2} (T_2^* - T_2) \\ &\approx \frac{4g\nu(2 - \nu)\sigma T_m^3}{2p_2} \left[T_R \left(1 - \frac{y}{4a} \right) - \frac{f_o}{R} (\psi_1 - \psi_3) \right] \end{aligned} \quad (7)$$

where T_m is the observed mean temperature at $y=0$ and

$$T_2^* = T_m \left(1 - \frac{y}{4a} \right).$$

From the recent occultation measurements from Mariner IV, the surface pressure is about 4.1 to 5.7 mb and the mean temperature of the atmosphere is about $180 \pm 20K$ (Kliore et al, 1965) for an assumed 100 percent carbon dioxide. With the above information, we can determine the absorptivity of the "grey" Martian atmosphere. The absorptivity computed by House (1965) is about 0.16. Since in a grey tenuous atmosphere, the absorptivity depends very little on temperature, this value may be adopted here. However, parts of the Martian surface are probably covered by a layer of fine dust. The lowest layers of the atmosphere probably contain a certain amount of dust particles, which will increase the absorptivity slightly. Therefore, the absorptivity was increased to 0.18 in the present computations. With this assumption, the computed radiative equilibrium temperature at level 2 is about 179K which is close enough to the results of the occultation measurements. Therefore, within the limits of available knowledge, the application of the linear approximation to Equation (7) is justified. Now we define the zonally averaged means for the quantity $G(x,y,t)$ by

$$\bar{G}(y,t) = \frac{1}{L} \int_0^L G(x,y,t) dx \quad (8)$$

and its disturbance by

$$G_t'(x,y,t) = G(x,y,t) - \bar{G}(y,t). \quad (9)$$

Introducing these operators to Equations (1) to (3) and the equation of continuity, and then integrating the equations with respect to y , we have

$$\frac{\partial \bar{u}_1}{\partial t} - f_o \bar{v}_1 = - \frac{\partial}{\partial y} (\bar{u}' v_1') + A \frac{\partial^2 \bar{u}_1}{\partial y^2} - k_i (\bar{u}_1 - \bar{u}_3) \quad (10)$$

$$\frac{\partial \bar{u}_3}{\partial t} - f_o \bar{v}_3 = - \frac{\partial}{\partial y} (\bar{u}_3' v_3') + A \frac{\partial^2 \bar{u}_3}{\partial y^2} + k_i (\bar{u}_1 - \bar{u}_3) - K \left(\frac{3}{2} \bar{u}_1 - \frac{\bar{u}_3}{2} \right) \quad (11)$$

$$\begin{aligned} f_o \frac{\bar{\omega}_2}{p_2} = & \lambda^2 \left[\frac{\partial}{\partial t} (\bar{\psi}_1 - \bar{\psi}_3) + \frac{\partial}{\partial y} \overline{v_2' (\psi_1' - \psi_3')} - \frac{R}{f_o c_p} \frac{dQ_2}{dt} - \right. \\ & \left. - A \frac{\partial^2}{\partial y^2} (\bar{\psi}_1 - \bar{\psi}_3) \right] \end{aligned} \quad (12)$$

and

$$\frac{\bar{\omega}_2}{p_2} = \frac{\partial \bar{v}_3}{\partial y} = - \frac{\partial \bar{v}_1}{\partial y} . \quad (13)$$

In the case of a steady symmetrical regime, the first three equations of the last set can be simplified to

$$-f_o \bar{v}_1 = AD^2 \bar{u}_1 - k_i (\bar{u}_1 - \bar{u}_3) \quad (14)$$

$$-f_o \bar{v}_3 = AD^2 \bar{u}_3 + k_i (\bar{u}_1 - \bar{u}_3) - K \left(\frac{3}{2} \bar{u}_1 - \frac{1}{2} \bar{u}_3 \right) \quad (15)$$

$$f_o \frac{\bar{\omega}_2}{p_2} = - \frac{\lambda^2 R}{f_o c_p} \frac{dQ_2}{dt} + \lambda^2 A \frac{\partial (\bar{u}_1 - \bar{u}_3)}{\partial y} \quad (16)$$

where

$$D^2 = \frac{d^2}{dy^2} .$$

From Equations (7), (13), and (16), we have

$$AD^4 \bar{u}_1 - (k_i + \lambda^2 A) D^2 (\bar{u}_1 - \bar{u}_3) + \frac{f_o^2 \Lambda}{RT_m} (\bar{u}_1 - \bar{u}_3) = \frac{f_o \Lambda}{4a} . \quad (17)$$

From (14) and (15) we arrive at

$$(D^2 + \frac{K}{2A}) \bar{u}_1 = - (D^2 - \frac{3K}{2A}) \bar{u}_3 \quad (18)$$

Eliminating \bar{u}_3 between (17) and (18), we obtain a sixth order, ordinary, non-homogeneous differential equation

$$\left[D^6 - \left(\frac{3K}{2A} + \frac{2K_i}{A} \right) D^4 + \left(\frac{KK_i}{A^2} + \frac{2f_o^2 \Lambda}{RT_m A} \right) D^2 - \frac{f_o^2 \Lambda K}{A^2 RT_m} \right] \bar{u}_1 = \frac{3f_o \Lambda K}{8aA^2} \quad (19)$$

where

$$K_j = k_i + \lambda^2 A$$

$$\Lambda = \frac{4\lambda^2 R g \nu (2-\nu) \sigma T_m^4}{2f_o c_p p_2^2} .$$

Six boundary conditions are needed, namely:

$$\bar{u}_1 = 0 \quad \text{at } y = \pm W \quad (20)$$

$$\bar{u}_3 = 0 \quad \text{at } y = \pm W \quad (21)$$

$$\text{and} \quad \bar{v}_1 = 0 \quad \text{at } y = \pm W \quad (22)$$

where $y = 0$ represents the position at $\pm 45^\circ$ latitude,
 $y = \pm W$ represents the positions at the pole and the equator respectively.

From Equations (14), (20), (21), and (22), we obtain the following conditions.

$$D^2 \bar{u}_1 = 0 \quad (23)$$

By using Equations (17), (18), (20), (21), and (23), we obtain

$$(AD^4) \bar{u}_1 = \frac{f_o \Lambda}{4a} \quad (24)$$

Finally, the six boundary conditions for u_1 can be rewritten as

$$\bar{u}_1 = 0 \quad \text{at } y = \pm W \quad (20)$$

$$D^2 \bar{u}_1 = 0 \quad \text{at } y = \pm W \quad (23)$$

$$D^4 \bar{u}_1 = \frac{f_o \Lambda}{4aA} \quad \text{at } y = \pm W \quad (24)$$

1.3 Solutions

The particular solution for Equation (19) is $\frac{3RT_m}{8af_o}$ and the complementary function of Equation (19) can be written as

$$\sum \alpha_\ell \exp(\beta_\ell y) \quad .$$

The complete solution is then

$$\sum_{\ell=1}^6 \alpha_\ell \exp(\beta_\ell y) + \frac{3RT_m}{8af_o} \quad (25)$$

The quantity β_ℓ can be obtained by, first, substituting $\exp(\beta_\ell y)$ into (19) and then solving the six-degree algebraic equation in β_ℓ . However, the six-degree algebraic equation can be reduced to a cubic equation and solved rather easily. When all values of β_ℓ are determined, α_ℓ can be determined from the boundary conditions (20), (23), and (24) through a six by six matrix operation.

If the three pairs of β_ℓ are one real and two complex conjugate roots, one can prove that the real part of the solution of α_ℓ should be four real negative numbers. The imaginary part of the solution of α_ℓ should add to zero. All these characteristics of the roots are attributed to the properties of the boundary conditions and the sixth order differential equation. These characteristics are very useful for checking the numerical results.

Suppose

$$\alpha_\ell = \alpha_{\ell 1} + \alpha_{\ell 2} i$$

$$\beta_\ell = a_\ell + b_\ell i \quad .$$

Then from (25), we have

$$\bar{u}_1 = \sum_{\ell=1}^{\ell=6} (\alpha_{\ell 1} + \alpha_{\ell 2} i) \exp(a_\ell y) (\cos b_\ell y + i \sin b_\ell y) + \frac{3RT_m}{8af_o} \quad . \quad (26)$$

The real part of the solution of \bar{u}_1 is

$$\text{Re } \bar{u}_1 = \sum_{\ell=1}^6 (\alpha_{\ell 1} \cos b_\ell y - \alpha_{\ell 2} \sin b_\ell y) \exp(a_\ell y) + \frac{3RT_m}{8af_o} \quad . \quad (27)$$

Substituting the solution (26) into Equation (18) we find the particular solution of \bar{u}_3 as

$$\frac{RT_m}{8af_o} - \sum_{\ell=1}^6 \frac{\alpha_\ell (\beta_\ell^2 + \frac{K}{2A})}{\beta_\ell^2 - \frac{3K}{2A}} \exp(\beta_\ell y)$$

and the complementary function as $a \exp(\gamma_1 y) + b \exp(-\gamma_1 y)$, where

$$\gamma_1 = \sqrt{\frac{3K}{2A}} \quad .$$

From the boundary condition on \bar{u}_3 we find

$$a = \frac{1}{\sinh 2\gamma_1 W} \left[\sum_{\ell=1}^6 \alpha_{\ell} \left(\frac{\beta_{\ell}^2 + \frac{K}{2A}}{\beta_{\ell}^2 - \frac{3K}{2A}} \right) \sinh (\beta_{\ell} + \gamma_1) W - \left(\frac{RT_m}{8af_o} \right) \cdot \sinh \gamma_1 W \right]$$

$$b = \frac{1}{\sinh 2\gamma_1 W} \left[\sum_{\ell=1}^6 \alpha_{\ell} \left(\frac{\beta_{\ell}^2 + \frac{K}{2A}}{\beta_{\ell}^2 - \frac{3K}{2A}} \right) \sinh (\gamma_1 - \beta_{\ell}) W - \left(\frac{RT_m}{8af_o} \right) \cdot \sinh \gamma_1 W \right] .$$

The real part of the solution for \bar{u}_3 is

$$\begin{aligned} \text{Re } \bar{u}_3 = & \frac{RT_m}{8af_o} - \frac{RT_m}{4af_o} \frac{\sinh \gamma_1 W}{\sinh 2\gamma_1 W} \cosh \gamma_1 y + \sum_{\ell=1}^6 \frac{1}{[(a_{\ell}^2 - b_{\ell}^2 - \frac{3K}{2A})^2 + 4a_{\ell}^2 b_{\ell}^2]} \cdot \\ & \cdot \left\{ \left[\alpha_{\ell 1} \left((a_{\ell}^2 - b_{\ell}^2 + \frac{K}{2A})(a_{\ell}^2 - b_{\ell}^2 - \frac{3K}{2A}) + 4a_{\ell}^2 b_{\ell}^2 \right) + \alpha_{\ell 2} \frac{4a_{\ell} b_{\ell} K}{A} \right] \cdot \right. \\ & \cdot \left[\left(\frac{1}{\sinh 2\gamma_1 W} \cdot (\sinh [a_{\ell} + \gamma_1] W \cdot \cos b_{\ell} W \exp[\gamma_{\ell} y] + \right. \right. \\ & \left. \left. + \sinh [\gamma_1 - a_{\ell}] W \cdot \cos b_{\ell} W \exp[-\gamma_1 y]) - \exp(a_{\ell} y) \cos b_{\ell} y \right) \right] - \\ & - \left[-\alpha_{\ell 1} \frac{4a_{\ell} b_{\ell} K}{A} + \alpha_{\ell 2} \left((a_{\ell}^2 - b_{\ell}^2 + \frac{K}{2A})(a_{\ell}^2 - b_{\ell}^2 - \frac{3K}{2A}) + 4a_{\ell}^2 b_{\ell}^2 \right) \right] \cdot \\ & \cdot \left[\frac{1}{\sinh 2\gamma_1 W} \left(\cosh (a_{\ell} + \gamma_1) W \cdot \sin b_{\ell} W \exp(\gamma_1 y) - \right. \right. \\ & \left. \left. - \cosh (\gamma_1 - a_{\ell}) W \cdot \sin b_{\ell} W \exp(-\gamma_1 y) \right) - \exp(a_{\ell} y) \sin b_{\ell} y \right] \left. \right\} \quad (28) \end{aligned}$$

Substituting (26), (27), and (28) into (14) we obtain the real part of \bar{v}_1 as

$$\begin{aligned} \text{Re } \bar{v}_1 = & \left(-\frac{A}{f_o} \right) \sum_{\ell=1}^6 \left\{ \left[\left(\alpha_{\ell 1} (a_{\ell}^2 - b_{\ell}^2) - 2a_{\ell} b_{\ell} \alpha_{\ell 2} \right) \cos b_{\ell} y - \left(\alpha_{\ell 2} (a_{\ell}^2 - b_{\ell}^2) + \right. \right. \right. \\ & \left. \left. \left. + 2a_{\ell} b_{\ell} \alpha_{\ell 1} \right) \sin b_{\ell} y \right] \exp(a_{\ell} y) \right\} + \frac{k_i}{f_o} (\bar{u}_1 - \bar{u}_3) . \end{aligned} \quad (29)$$

Taking the derivative of (29) with respect to y and using the approximation

$$w_2 \approx -\frac{\omega}{\rho g}$$

we have

$$\begin{aligned} \text{Re } \bar{w}_2 \approx -\frac{\omega_2}{\rho g} = & \frac{RT}{g} \left(-\frac{k_i}{f_o} \right) \sum_{\ell=1}^6 \frac{1}{(a_{\ell}^2 - b_{\ell}^2 - \frac{3K}{2A})^2 + 4a_{\ell}^2 b_{\ell}^2} \left\{ \left[\alpha_{\ell 1} \left((a_{\ell}^2 - b_{\ell}^2 + \frac{K}{2A}) \cdot \right. \right. \right. \\ & \cdot (a_{\ell}^2 - b_{\ell}^2 - \frac{3K}{2A}) + 4a_{\ell}^2 b_{\ell}^2 \left. \right) + \alpha_{\ell 2} \frac{4a_{\ell} b_{\ell} K}{A} \left. \right] \left[\frac{\gamma_1 \cos b_{\ell} W}{\sinh 2\gamma_1 W} \cdot \right. \\ & \cdot \left(\sinh (a_{\ell} + \gamma_1) W \cdot \exp(\gamma_1 y) - \sinh (\gamma_1 - a_{\ell}) W \cdot \exp(-\gamma_1 y) \right) - \\ & - \left(a_{\ell} \cos b_{\ell} y - b_{\ell} \sin b_{\ell} y \right) \exp(a_{\ell} y) \left. \right] - \left[-\alpha_{\ell 1} \frac{4a_{\ell} b_{\ell} K}{A} + \right. \\ & + \alpha_{\ell 2} \left((a_{\ell}^2 - b_{\ell}^2 + \frac{K}{2A}) (a_{\ell}^2 - b_{\ell}^2 - \frac{3K}{2A}) + 4a_{\ell}^2 b_{\ell}^2 \right) \left. \right] \left[\frac{\gamma_1 \sin b_{\ell} W}{\sinh 2\gamma_1 W} \cdot \right. \\ & \cdot \left(\cosh (a_{\ell} + \gamma_1) W \cdot \exp(\gamma_1 y) + \cosh (\gamma_1 - a_{\ell}) W \cdot \exp(-\gamma_1 y) \right) - \\ & - \exp(a_{\ell} y) \left(a_{\ell} \sin b_{\ell} y + b_{\ell} \cos b_{\ell} y \right) \left. \right] \left. \right\} + \sum_{\ell=1}^6 \left\{ \left[\left(-\frac{A}{f_o} \right) \cdot \right. \right. \\ & \cdot \left(\alpha_{\ell 1} (a_{\ell}^3 - 3a_{\ell} b_{\ell}^2) - \alpha_{\ell 2} (3a_{\ell}^2 b_{\ell} - b_{\ell}^3) \right) + \frac{k}{f_o} \left(\alpha_{\ell 1} a_{\ell} - \alpha_{\ell 2} b_{\ell} \right) \left. \right] \cdot \end{aligned}$$

$$\begin{aligned}
& \cdot \cos b_{\ell} y - \left[\left(-\frac{A}{f_o} \right) \left(\alpha_{\ell 1} (3a_{\ell}^2 b_{\ell} - b_{\ell}^3) + \alpha_{\ell 2} (a_{\ell}^3 - 3a_{\ell} b_{\ell}^2) \right) + \right. \\
& \left. + \frac{k_i}{f_o} \left(\alpha_{\ell 1} b_{\ell} + a_{\ell} \alpha_{\ell 2} \right) \right] \sin b_{\ell} y \} \exp(a_{\ell} y) + \frac{k_i}{f_o} \frac{\gamma_1 R T_m}{4a f_o} \cdot \\
& \cdot \frac{\sinh \gamma_1 W}{\sinh 2\gamma_1 W} \sinh \gamma_1 y \Bigg) \cdot \quad (30)
\end{aligned}$$

Equations (27) and (28) are the equations used for computing the mean zonal velocities at levels 1 and 3 as a function of latitude. Equation (29) is used to compute the mean meridional velocity at level 1. Equation (30) is the expression for the mean vertical velocity in pressure units at level 2.

The symmetrical circulation regime accomplishes a reduction in the radiative equilibrium temperature difference between equator and pole. The reduction is simply

$$\begin{aligned}
\Delta T &= (T_2^* - T_2)^{-W} \\
&= \left[T_m \left(1 - \frac{y}{4a} \right) - \frac{f_o}{R} \int \left(\bar{u}_1 - \bar{u}_3 \right) dy \right]^{-W} \cdot \quad (31)
\end{aligned}$$

After evaluating the integral, one obtains the real part of ΔT as

$$\begin{aligned}
\text{Re } \Delta T &= \frac{2f_o}{R\gamma_1} \left\{ \frac{\sinh \gamma_1 W}{\sinh 2\gamma_1 W} \sum_{\ell=1}^6 \frac{1}{[(a_{\ell}^2 - b_{\ell}^2 - \frac{3K}{2A})^2 + 4a_{\ell}^2 b_{\ell}^2]} \left[\alpha_{\ell 1} \left((a_{\ell}^2 - b_{\ell}^2 + \frac{K}{2A})(a_{\ell}^2 - b_{\ell}^2 - \frac{3K}{2A}) + \right. \right. \right. \\
& \left. \left. + 4a_{\ell}^2 b_{\ell}^2 \right) + \alpha_{\ell 2} \left(\frac{4a_{\ell} b_{\ell} K}{A} \right) \right] \left[\left(\sinh (a_{\ell} + \gamma_1)W + \sinh (\gamma_1 - a_{\ell})W \right) \cdot \right. \\
& \left. \cdot \cos b_{\ell} W \right] - \left[-\alpha_{\ell 1} \frac{4a_{\ell} b_{\ell} K}{A} + \alpha_{\ell 2} \left((a_{\ell}^2 - b_{\ell}^2 + \frac{K}{2A})(a_{\ell}^2 - b_{\ell}^2 - \frac{3K}{2A}) + 4a_{\ell}^2 b_{\ell}^2 \right) \right] \cdot \\
& \cdot \left[\left(\cosh (a_{\ell} + \gamma_1)W - \cosh (\gamma_1 - a_{\ell})W \right) \sin b_{\ell} W \right] \Bigg\} - \frac{2f_o}{R} \sum_{\ell=1}^6 \cdot \\
& \cdot \left\{ \frac{2(a_{\ell}^2 - b_{\ell}^2) - \frac{K}{A}}{(a_{\ell}^2 + b_{\ell}^2) [(a_{\ell}^2 - b_{\ell}^2 - \frac{3K}{2A})^2 + 4a_{\ell}^2 b_{\ell}^2]} \left[\left(\alpha_{\ell 1} a_{\ell} + \alpha_{\ell 2} b_{\ell} \right) \cdot \right. \right.
\end{aligned}$$

$$\begin{aligned}
& \cdot \left(\sinh a_\ell W \cos b_\ell W \left(a_\ell^2 - b_\ell^2 - \frac{3K}{2A} \right) + 2a_\ell b_\ell \cosh a_\ell W \sin b_\ell W \right) - \\
& - \left(\alpha_{\ell 2} a_\ell - \alpha_{\ell 1} b_\ell \right) \left((-2a_\ell b_\ell) \sinh a_\ell W \cos b_\ell W + \left(a_\ell^2 - b_\ell^2 - \frac{3K}{2A} \right) \cdot \right. \\
& \cdot \left. \left(\cosh a_\ell W \sin b_\ell W \right) \right] - \frac{4a_\ell b_\ell}{(a_\ell^2 + b_\ell^2) \left[\left(a_\ell^2 - b_\ell^2 - \frac{3K}{2A} \right)^2 + 4a_\ell^2 b_\ell^2 \right]} \cdot \\
& \cdot \left[\left(\alpha_{\ell 2} a_\ell - \alpha_{\ell 1} b_\ell \right) \left(\sinh a_\ell W \cos b_\ell W \left(a_\ell^2 - b_\ell^2 - \frac{3K}{2A} \right) + \right. \right. \\
& + 2a_\ell b_\ell \cosh a_\ell W \sin b_\ell W \left. \right) + \left(\alpha_{\ell 1} a_\ell + \alpha_{\ell 2} b_\ell \right) \left((-2a_\ell b_\ell) \sinh a_\ell W \cdot \right. \\
& \cdot \left. \cos b_\ell W + \left(a_\ell^2 - b_\ell^2 - \frac{3K}{2A} \right) \cosh a_\ell W \sin b_\ell W \right) \left. \right] \left. \right\} - \\
& - \frac{T_m}{4a\gamma_1} \frac{\sinh^2 \gamma_1 W}{\sinh 2\gamma_1 W} \cdot
\end{aligned} \tag{32}$$

The results of the computations are discussed in the next section.

1.4 Results and Discussion

In order to compute the wind velocities and the reduction in the radiative temperature difference between equator and pole accomplished by the circulation, we have to know the factor λ^2 . The factor is a function of $\theta_2/(\theta_1 - \theta_3)$ and is a measure of the static stability of the atmosphere. The potential temperatures θ_1 , θ_2 , and θ_3 at levels 1, 2, and 3 for Mars can be determined from estimates of the vertical temperature profile. With the convective-radiative equilibrium model of Ohring and Mariano (1965) and composition and pressure data from the results of the Martian IV occultation experiment, the vertical temperature profile can be estimated theoretically. The following input parameters are assumed: surface temperature is 217°K; g is 373 cm/sec²; c_p is 0.203 cal gm⁻¹ deg⁻¹; c_p/c_v is 1.28; R is 1.89 x 10⁶ cm² sec⁻² deg⁻¹ and an adiabatic lapse rate is assumed in troposphere. The computed temperature profile is shown in Figure 1.

From this profile we compute the quantity $\theta_2/(\theta_1 - \theta_3)$, which is about 46. The corresponding values of λ^2/k_i and Λ/k_i for f_o of 0.9×10^{-4} sec⁻¹ are shown in Table 1.

TABLE 1
Values of λ^2/k_i and Λ/k_i for different μ .

μ (gm cm ⁻¹ sec ⁻¹)	$\frac{\lambda^2}{k_i} \left(= \frac{P_2 f_o^2}{\mu g} \frac{\theta_2}{\theta_1 - \theta_3} \right)$ (cm ⁻² sec)	$\frac{\Lambda}{k_i} \left(= \frac{R g \nu (2 - \nu) \sigma T_m^4}{\mu g c_p} \frac{\theta_2}{\theta_1 - \theta_3} \right)$
50	0.13×10^{-9}	21
100	0.65×10^{-10}	10.5
200	0.38×10^{-10}	5.3

In Table 1, the absorptivity ν is assumed to be 0.18; the temperature T_m is assumed to be 185°K. k_i may be written as

$$k_i = \frac{\mu g^2}{R T_2 P_2} \quad (33)$$

The quantity Λ can be computed by multiplying k_i by the value $\frac{\Lambda}{k_i}$ in Table 1 and is

$$\Lambda = 10.01 \times 10^{-5} \text{ sec}^{-1}.$$

The quantity K_j can also be computed from the following formula if A and μ are given

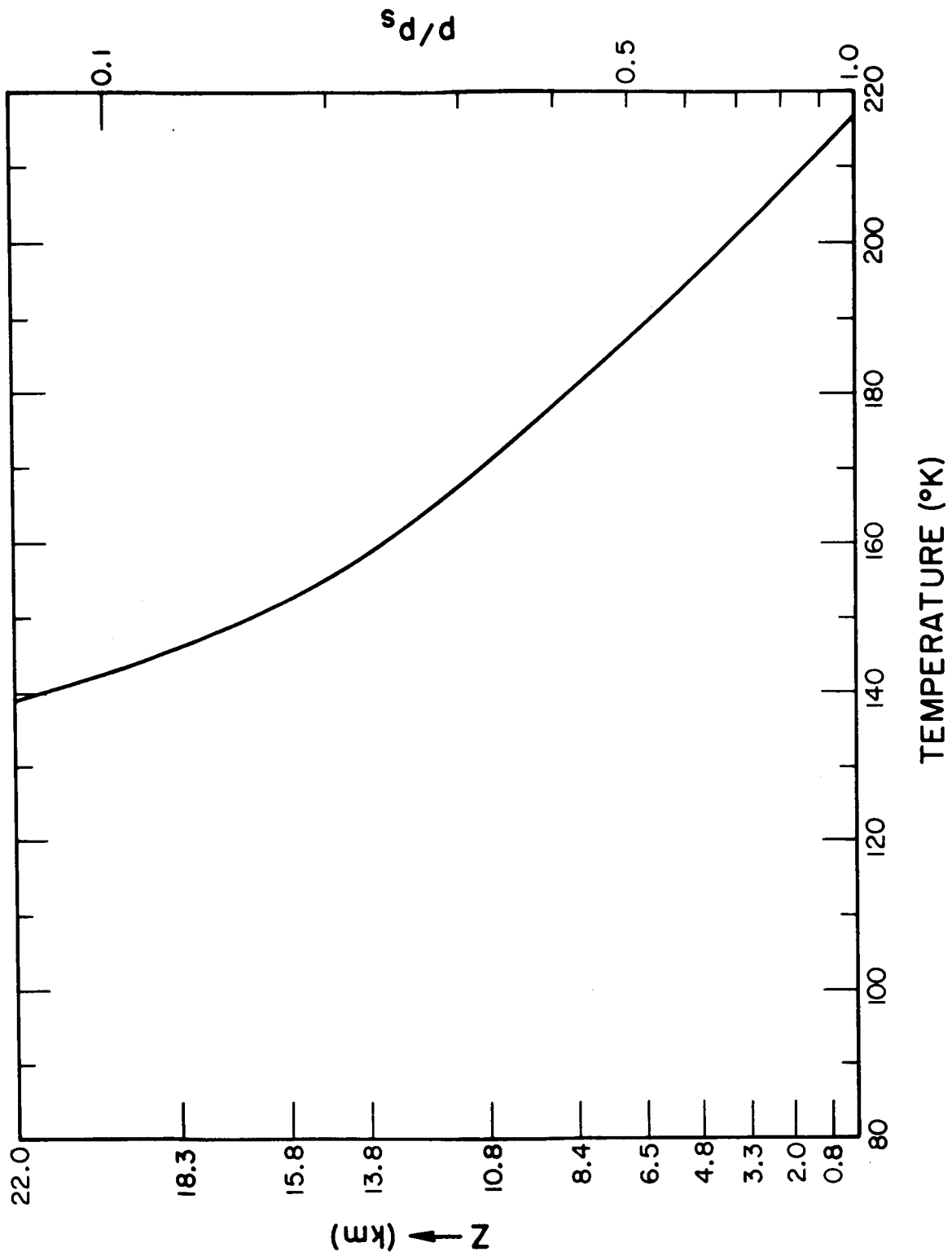


Figure 1. Vertical temperature profile for Martian atmosphere.

$$\begin{aligned}
K_j &= k_i + \lambda^2 A = k_i \left(1 + \frac{p_2 f_o^2}{\mu g^2} \frac{\theta_2}{\theta_1 - \theta_3} A \right) \\
&= k_i \left(1 + 3.63 \times 10^{-9} \frac{A}{\mu} \right)
\end{aligned}
\tag{34}$$

The values of K_j for different A and μ are shown in Table 2.

TABLE 2

Values of K_j for different lateral eddy viscosities, and vertical coefficients of dynamic eddy viscosity μ .

$A(\text{cm}^2 \text{ sec}^{-1})$	$\mu(\text{gm cm}^{-1} \text{ sec}^{-1})$	$K_j \text{ (sec}^{-1}\text{)}$
10^9	50	0.81×10^{-5}
	100	1.54×10^{-5}
	200	2.99×10^{-5}
10^{10}	50	1.66×10^{-5}
	100	2.38×10^{-5}
	200	3.97×10^{-5}
10^{11}	50	10.08×10^{-5}
	100	10.80×10^{-5}
	200	13.8×10^{-5}

Another constant, K , in the expression of the surface stress is adapted as $4 \times 10^{-6} \text{ sec}^{-1}$ (Phillips, 1956).

The computed mean velocities at different levels based on the above input data for various lateral eddy viscosities, A , and vertical coefficients of eddy viscosity μ , are shown in Figures 2 to 10. \bar{u}_1 , \bar{u}_2 , and \bar{u}_3 are the mean zonal winds at levels 1, 2, and 3. \bar{u}_1 and \bar{u}_3 are computed from Equations 27 and 28 and values of \bar{u}_2 are interpolated; \bar{v}_1 , the mean meridional wind at level 1, is computed from Equation 29.

01GA97-10F

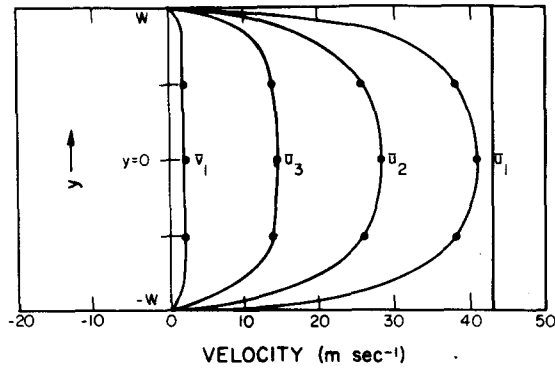


Figure 2. Mean zonal and meridional wind velocities for the case of $A = 10^9 \text{ cm}^2 \text{ sec}^{-1}$ and $\mu = 50 \text{ gm cm}^{-1} \text{ sec}^{-1}$.

01GA97-40F

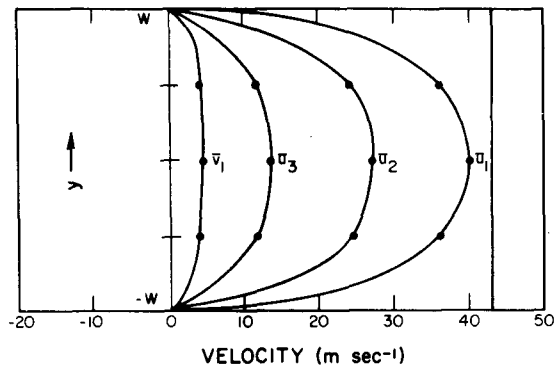


Figure 3. Mean zonal and meridional wind velocities for the case of $A = 10^9 \text{ cm}^2 \text{ sec}^{-1}$ and $\mu = 100 \text{ gm cm}^{-1} \text{ sec}^{-1}$.

01GA97-30F

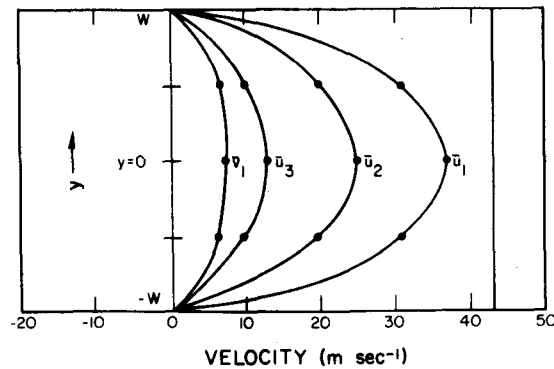


Figure 4. Mean zonal and meridional wind velocities for the case of $A = 10^9 \text{ cm}^2 \text{ sec}^{-1}$ and $\mu = 200 \text{ gm cm}^{-1} \text{ sec}^{-1}$.

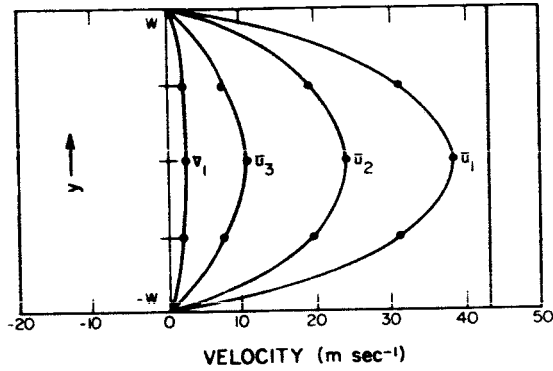


Figure 5. Mean zonal and meridional wind velocities for the case of $A = 10^{10} \text{ cm}^2 \text{ sec}^{-1}$ and $\mu = 50 \text{ gm cm}^{-1} \text{ sec}^{-1}$.

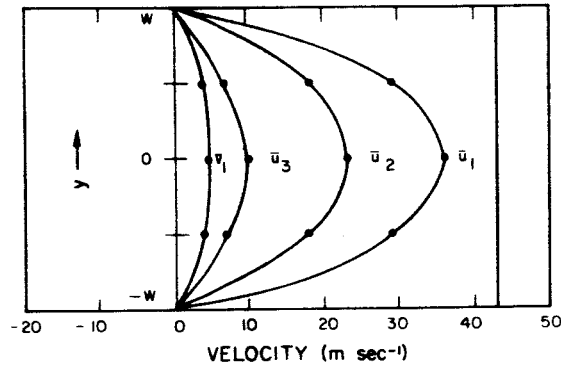


Figure 6. Mean zonal and meridional wind velocities for the case of $A = 10^{10} \text{ cm}^2 \text{ sec}^{-1}$ and $\mu = 100 \text{ gm cm}^{-1} \text{ sec}^{-1}$.

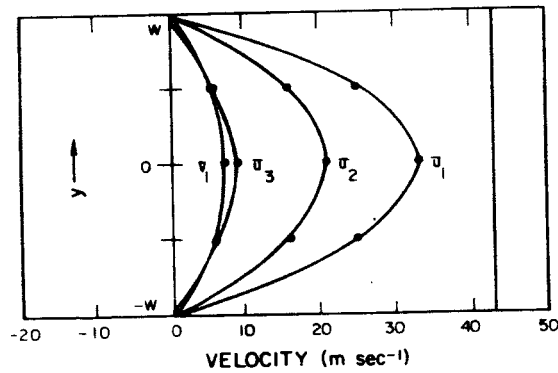


Figure 7. Mean zonal and meridional wind velocities for the case of $A = 10^{10} \text{ cm}^2 \text{ sec}^{-1}$ and $\mu = 200 \text{ gm cm}^{-1} \text{ sec}^{-1}$.

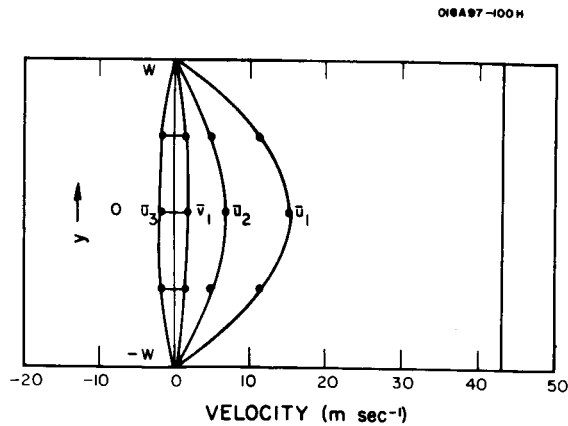


Figure 8. Mean zonal and meridional wind velocities for the case of $A = 10^{11} \text{ cm}^2 \text{ sec}^{-1}$ and $\mu = 50 \text{ gm cm}^{-1} \text{ sec}^{-1}$.

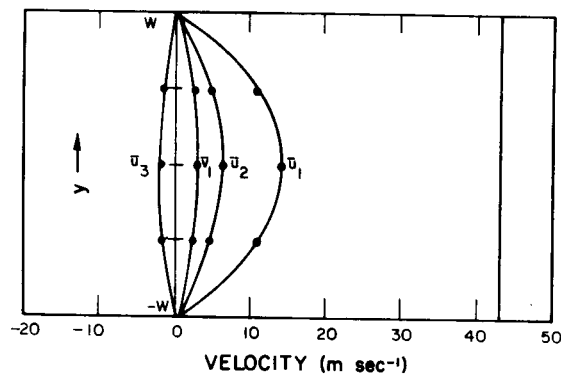


Figure 9. Mean zonal and meridional wind velocities for the case of $A = 10^{11} \text{ cm}^2 \text{ sec}^{-1}$ and $\mu = 100 \text{ gm cm}^{-1} \text{ sec}^{-1}$.

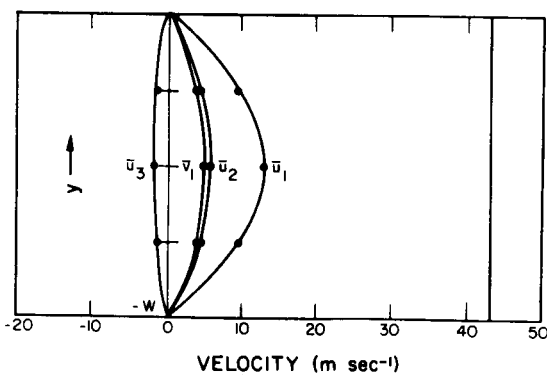


Figure 10. Mean zonal and meridional wind velocities for the case of $A = 10^{11} \text{ cm}^2 \text{ sec}^{-1}$ and $\mu = 200 \text{ gm cm}^{-1} \text{ sec}^{-1}$.

The mean meridional wind velocities, \bar{v}_3 , at level 3 are not shown in these figures, but they have the same magnitude as \bar{v}_1 and are of opposite sign.

From the mean zonal winds at levels 1 and 3, we can estimate the mean zonal winds at level 4 by extrapolation from an assumed linear profile. The results are shown in Figure 11.

As can be seen from Figures 2 to 11, the different values of A and μ produce different wind profiles. As A increases, the maximum zonal wind velocities at middle latitudes decrease. For $A < 10^{10} \text{ cm}^2 \text{ sec}^{-1}$, the change is small. For $A = 10^{11} \text{ cm}^2 \text{ sec}^{-1}$, the wind velocity at level 1 reduces to about one half the value for $A = 10^{10} \text{ cm}^2 \text{ sec}^{-1}$. When $A = 10^9 \text{ cm}^2 \text{ sec}^{-1}$, the meridional wind profiles are flatter in middle latitudes than those for larger A .

The small deviations of the mean zonal wind speeds between the cases $A = 10^9 \text{ cm}^2/\text{sec}$ and $A = 10^{10} \text{ cm}^2/\text{sec}$ is due to the fact that the magnitude of the lateral friction is assumed smaller than the magnitude of the vertical friction. Therefore, neglect of the lateral friction has little influence on the maximum magnitude of the mean zonal wind. However, when $A \gg 10^{10} \text{ cm}^2/\text{sec}$, the magnitude of lateral friction dominates over vertical friction. As a consequence, not only is the magnitude of the mean zonal wind at level 1 sharply reduced, but also the mean zonal wind direction at level 3 changes from west to east. For the case of zero vertical frictional stress, an east wind must be found at the level 3. This can be very easily seen from Equation (18). This phenomenon will also be found in the general circulation model developed from Bjerknes' circulation theorem when surface friction is not taken into account. This may be explained physically as follows. When large scale geostrophic balance is reached in the atmosphere, in which the temperature is higher at the equator than at the pole, the flows at levels 1 and 3 on a rotating planet, are west and east, respectively. Since an east wind means that the atmosphere is moving more slowly than the tangential velocity of the rotating planet at surface level, the east wind would be reduced by the drag of the planetary surface. The easterly component at higher levels will also be reduced due to internal friction. Finally, the wind at level 3 may be either a weak easterly wind or a westerly wind. Thus, with the inclusion of vertical friction, the westerly component of the wind at level 3 is increased.

The meridional wind speeds increase when the coefficient of vertical eddy viscosity, k_1 , increases. Mathematically, this can be seen from Equation (14). From the physical point of view, the increase of meridional velocity with the corresponding increase of vertical internal friction is attributed to the fact that the frictional force always causes the actual wind to flow across the contour lines toward "low" areas and to deviate from the geostrophic wind. The frictional force will upset the original force of balance between the pressure gradient force and the Coriolis force. A new balance of forces among the frictional force, the pressure gradient force, and the Coriolis force must be reached if friction is

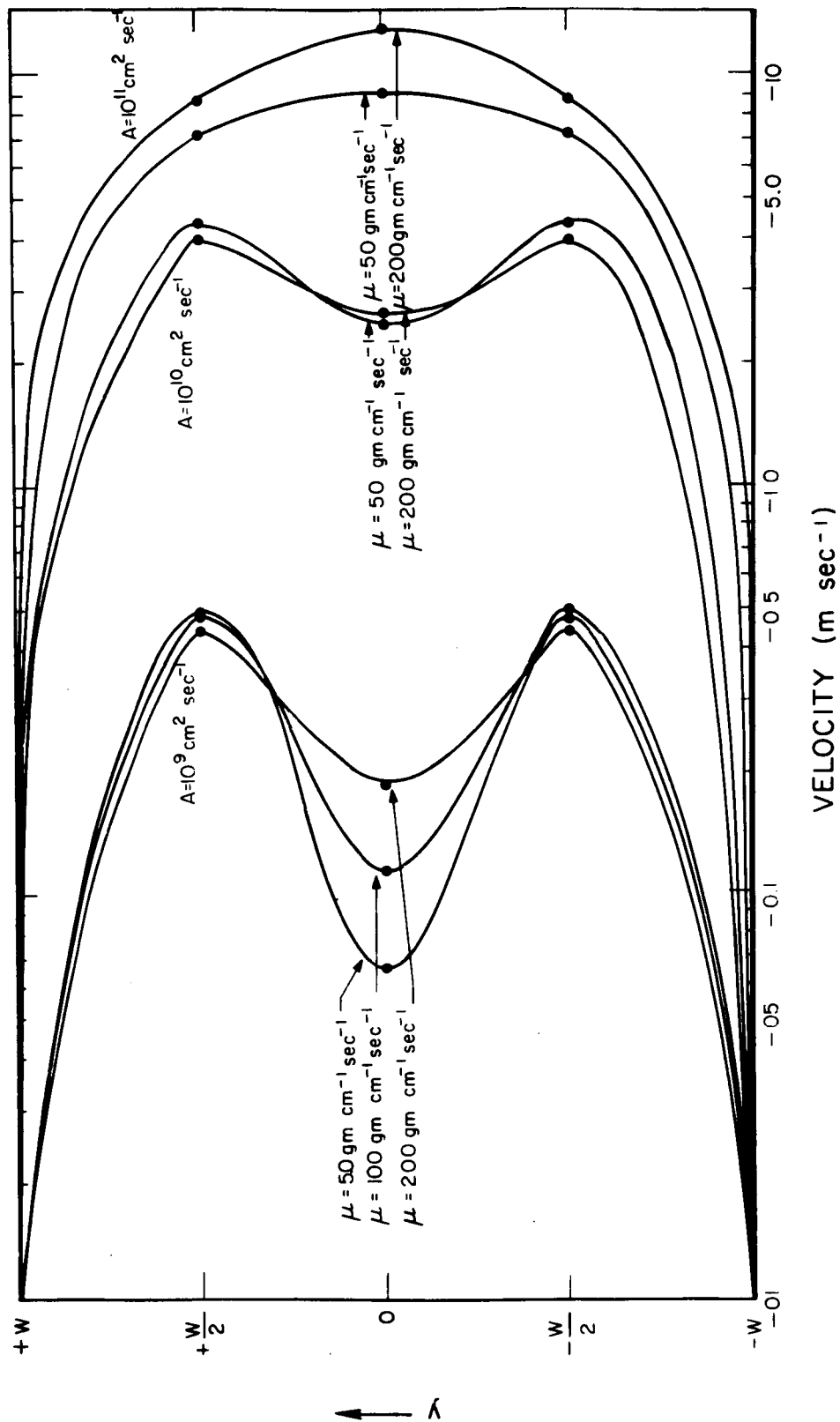


Figure 11. Mean surface wind velocities for various lateral eddy viscosities, A , and vertical coefficients of eddy viscosity, μ , extrapolated from mean wind velocities at levels 1 and 3.

introduced or increased. As a result of this new balance, the component of the wind directed toward lower pressures will be increased. In the upper layer of the atmosphere, the geopotential height is higher at lower latitudes than at high latitudes. Therefore, the northward component of wind will increase if the vertical internal friction is higher.

For the completely frictionless case, $\mu = k_i = K = A = 0$, the governing equation, (19), reduces to

$$\bar{u}_1 = \frac{3RT_m}{8af_0} \quad (35)$$

For numerical values of T_m , R , a , and f_0 as shown before, \bar{u}_1 is about 43 m/sec. It may be worthwhile to mention here that this quantity is $\frac{3}{2}$ times that based on Charney's (1959) formula. The cause of this difference is due to the somewhat different form of the surface stress used in our computations. We assume the surface stress to be proportional to the first power of the surface wind, as also assumed by Phillips (1956). To compute the surface stress, a value for the surface wind is required. Since surface wind is not directly computed from the equations, a linear extrapolation is made downward from levels 1 and 3, so that u_4 is written as

$$\bar{u}_4 = \frac{3}{2} \bar{u}_3 - \frac{\bar{u}_1}{2}$$

In Charney's approach however, \bar{u}_4 is further simplified by assuming

$$\bar{u}_4 = \frac{1}{2} \bar{u}_3$$

This approximation, when introduced into the equation of motion, leads to a zero wind velocity at level 3, which is not a realistic velocity.

Figure 11 shows the zonal wind at level 4, the level near the surface. For $A = 10^{10} \text{ cm}^2 \text{ sec}^{-1}$ or less, the zonal wind has a double peak, in contrast to the case of $A = 10^{11}$ or to the higher level winds, which all have single mid-latitude peaks. The values of the wind for these cases are small, however, and the double peak may be the result of using a simple linear extrapolation technique.

The theoretical values of zonal and meridional velocities at level 1 for the earth, computed by Charney (1959) without considering lateral friction, are about 24 m sec^{-1} and 12 cm sec^{-1} , respectively. A similar computation for earth with our model, with $A = 0$, yields a maximum zonal wind velocity at level 1 equal to about 36 m sec^{-1} . If the lateral eddy viscosity is taken into account, the estimated magnitude of the zonal wind would be somewhat reduced, depending upon the magnitude of A chosen. The choice of the right value of A for the free atmosphere is difficult. Based upon the empirical and theoretical studies by Richardson and Oboukhov (see Gandii, 1955) on the relation between the lateral eddy viscosity A , and the scale of motion

of a system, the quantity A may be written as

$$A \approx 10^{-2} L^{\frac{4}{3}} m^2 \text{ sec}^{-1}$$

For the scale of eddies of the general circulation in the terrestrial atmosphere

$$L \approx 2 \times 10^6 \text{ m} ,$$

and, hence, $A \approx 2.5 \times 10^{10} \text{ cm}^2 \text{ sec}^{-1}$. This value was used by Adem (1962) with some success. If $A = 10^{10} \text{ cm}^2 \text{ sec}^{-1}$ is used in our model to compute the wind velocity in the earth's atmosphere, the computed values at levels 1 and 3 are $\bar{u}_1 = 33 \text{ m sec}^{-1}$ and $\bar{u}_3 = 10 \text{ m sec}^{-1}$. The mean zonal velocity, \bar{u}_1 , at level 1 in middle latitudes of the Northern and Southern Hemisphere on Earth in summer and winter (based upon Obasi, 1963) are shown in Table 3.

TABLE 3

Mean zonal wind velocities between 30° and 60° latitude in the terrestrial atmosphere, calculated from the results reported by Obasi (1963).

Hemisphere	Mean Zonal Wind Velocities (m sec^{-1})					
	250 mb			750 mb		
	Summer	Winter	Yearly Mean	Summer	Winter	Yearly Mean
Northern Hemisphere	13	17	15	3	6	5
Southern Hemisphere	22	26	24	8	10	9
Mean			20			7

The observed and computed values are in reasonable agreement. Therefore, $A = 10^{10} \text{ cm}^2 \text{ sec}^{-1}$ is probably a proper value for the earth's atmosphere.

What is the most probable value of A for Mars? No one really knows. A reasonable estimate might be a value similar to that in the earth's atmosphere - $A = 10^{10} \text{ cm}^2 \text{ sec}^{-1}$.

For $A = 10^{10} \text{ cm}^2 \text{ sec}^{-1}$ and $\mu = 100 \text{ gm cm}^{-1} \text{ sec}^{-1}$, the Martian mean zonal and meridional velocities at middle latitude at different levels are shown in Table 4.

TABLE 4

The Martian mean zonal and meridional at middle latitudes at different levels (+ represents west or south wind, - represents north or east wind).

level	Mean Zonal Velocities (m/sec)	Meridional Velocities (m/sec)
1	36	5
2	24	0
3	10	-5
4	-2	-10

The computed meridional wind velocities for Mars as shown in Table 4 are on the average about one order of magnitude higher than those of the earth. Since the magnitude of the meridional wind velocity is almost linearly proportional to k_1 , and k_1 is inversely proportional to p_2 , as seen in Equation (33), the meridional wind velocity on a planet having a small surface pressure, will be larger. Thus, the large value of the meridional velocity on Mars may be attributed to the low surface pressure on the planet. The meridional velocities at levels 2 and 4 are obtained by linear interpolation and extrapolation, respectively. The magnitude of the meridional velocity at the surface level is 10 m sec^{-1} , which is several times the mean zonal velocity at the surface in the symmetrical regime. As shown later, a symmetrical circulation regime is not dominant on Mars and is replaced by a wave regime. We have no data here to show how the meridional velocities at different levels would change from symmetrical regime, when the wave regime is developed. However, it is highly probable that the high percentage of meridional cloud movements at low latitude on Mars (Gifford, 1965; Tang, 1965) is directly associated with the relatively strong mean meridional wind velocity and indirectly with the low value of the surface pressure on Mars.

The radiative equilibrium pole-to-equator temperature difference in this model is about 74°C. The temperature difference between pole and equator is reduced by an amount ΔT by the symmetrical circulation. The final pole-to-equator temperature difference, T_{pe} , is then

$$T_{pe} = 74^{\circ}\text{C} - \Delta T \quad (37)$$

where ΔT represents the reduction in the temperature difference that is produced by the symmetrical circulation. The calculated values of ΔT and T_{pe} for various A and μ are shown in Table 5.

TABLE 5

The calculated magnitude of the pole-to-equator temperature differences, T_{pe} at the middle of the Martian atmosphere of the symmetrical regime for various lateral eddy viscosities A , and vertical dynamic coefficients of eddy viscosity, μ .

$A(\text{cm}^2/\text{sec})$	$\mu(\text{gm/cm/sec})$	$\Delta T (^{\circ}\text{C})$	$T_{pe} (^{\circ}\text{C})$
10^9	50	14	60
	100	18	56
	200	25	49
10^{10}	50	21	53
	100	25	49
	200	30	44
10^{11}	50	50	24
	100	51	23
	200	54	20

Based upon observational inferences, the mean magnitude of pole-to-equator temperature difference at the surface is about 35°C to 40°C (Ohring, Tang, and DeSanto, 1962; Mintz, 1961). The mean magnitude of the pole-to-equator temperature difference at the middle of the atmosphere is probably less than this value - perhaps having a value of 25°C to 30°C. The computed magnitudes of the atmospheric pole-to-equator temperature

differences produced by the symmetrical circulation are greater than those inferred from observations, except when $A = 10^{11} \text{ cm}^2 \text{ sec}^{-1}$. For our best estimate of A ($= 10^{10} \text{ cm}^2 \text{ sec}^{-1}$) and μ ($= 100 \text{ gm cm}^{-1} \text{ sec}^{-1}$), the computed temperature difference, T_{pe} , is about 50°C , which is at least 20°C to 25°C higher than the observed value. This means that the observed average temperature difference cannot be explained by a symmetrical circulation regime. The symmetrical regime is not effective in transporting heat, and is therefore replaced by a wave regime, which is more efficient in transporting heat. The parameters used in these calculations are for the Martian equinoctial seasons, and, therefore, these conclusions are representative of the average Martian year.

Although the symmetrical regime is not the prevailing regime in the Martian atmosphere, the velocities computed above should be first approximations of the average zonal and meridional velocities of the atmosphere at middle latitudes.

As a continuation of this study, a non-steady, asymmetric model that includes time variations and eddy transports of zonal momentum will be developed and applied to Mars.

REFERENCES

- Adem, J., 1962: On the theory of the general circulation of the atmosphere. Tellus, 14, 102-115.
- Charney, J., 1959: On the general circulation of the atmosphere. The Atmosphere and the Sea in Motion. The Rockefeller Institute Press, New York, 509 pp.
- Gandii, L. S., 1955: Problems in Dynamic Meteorology Foundation. Hydro-meteorology Publication, USSR, 788 pp. (Chinese Translation Edition.)
- Gifford, F. A., Jr. 1964: A study of Martian yellow clouds that display movement. Mon. Wea. Rev., 92, 425-440.
- House, F., 1965: The seasonal climatology of Mars. In Planetary Meteorology Quart. Prog. Rpt. No. 2, Contract No. NASW-1227. GCA Corp., Bedford.
- Kliore, A., D.L. Cain, G.S. Levy, Von R. Eshleman, G. Fjeldbo, and F.D. Drake, 1965: Occultation experiment: Results of the first direct measurement of Mars' atmosphere and ionosphere. Science, 49, 1243-1248.
- Mintz, Y., 1961: The general circulation of planetary atmospheres. The Atmosphere of Mars and Venus. National Academy of Sciences, National Research Council Publication 44, 107-146.
- Obasi, G.O.P., 1963: Atmospheric momentum and energy calculations for the Southern Hemisphere during the IGY. Scientific Report No. 6, Planetary Circulation Project, M.I.T. under Contract AF19(604)-6108.
- Ohring, G., and J. Mariano, 1965: Study of the average vertical distribution of temperature in the Martian atmosphere. GCA Tech. Rpt. No. 65-3-N, under Contract No. NAS 9-3423.
- Ohring, G., W. Tang, and G. DeSanto, 1962: Theoretical estimates of the average surface temperature on Mars. J. Atmos. Sci., 19, 444-449.
- Phillips, N.A., 1956: The general circulation of the atmosphere: A numerical experiment. Quart. J. of the Royal Meteor. Soc., 82, 123-164.
- Tang, W., 1965: Some aspects of the atmospheric circulation on Mars. Tech. Rpt., GCA Corp., Bedford, Mass., under Contract No. NASw-975, NASA Contractor Report NASA CR-262, 43 pp.

2. THE SEASONAL CLIMATOLOGY OF MARS

Frederick B. House

2.1 Introduction

The climate on Mars has been a subject of debate since the invention of the telescope. The basis for a study of Martian climatology is the welding together of available observational data and appropriate theory. Prior to the early radiometric measurements of Mars by Coblentz and Lampland (1923), estimates of Martian climatology used visual and photographic observations in order to calculate surface and atmospheric temperatures, e.g., Milankovitch (1920). Gifford (1956) has summarized radiometric measurements of Mars over the years in a seasonal climatology of the surface temperature distribution. Measurements by Sinton and Strong (1960), and by Kaplan, Munch, and Spinrad (1964), have increased our knowledge about the diurnal temperature variation and composition of the Martian surface, and about the total pressure and composition of the atmosphere of Mars, respectively. Results from the radio occultation experiment during the Mariner IV fly-by of Mars (Kliore, et al, 1965) have added considerably to our knowledge of the Martian atmospheric pressure and composition. In light of these new measurements, a study of the seasonal variations of the Martian climate seems appropriate at this time.

Recent research emphasis has centered around investigations of the temperature structure of the Martian atmosphere, e.g., Goody (1957), Arking (1963), Ohring (1963), and Prabhakara and Hogan (1965). The results of these investigations are based on calculations using multi-layered model atmospheres which generally apply to the average Martian latitude and climate.

In this paper, a simple theoretical model is formulated to determine the latitudinal and seasonal variation of the surface and mean atmospheric temperatures of Mars. In this model, the temperature climate is computed from conditions of radiative equilibrium, assuming the atmosphere to be stationary. The spectral properties of the Martian atmosphere are assumed to be non-gray, that is, the absorptivity and emissivity of the atmosphere to thermal radiation are a function of the surface and atmospheric temperatures, respectively. The absorption of solar radiation by the atmosphere occurs in the near infrared bands of carbon dioxide and water vapor, and this absorption is assumed to be independent of atmospheric temperature. Gray spectral properties are assumed to hold for the absorption and emission of radiation at the surface.

In a climatological study such as this, the need for a model atmosphere which calculates a detailed vertical temperature structure is of secondary importance to the inferred climatic variations. Instead of using a sophisticated multi-layered model atmosphere, this study incorporates a single-layered atmosphere in order to reduce the computing time and to emphasize the changes in climate. The loss in accuracy when using the single-layered model is probably no greater than the error introduced by the uncertainty in total pressure and composition of the Martian atmosphere.

2.2 Radiative Equilibrium Model Atmosphere

In any planetary heat budget study, the fundamental law of energy conservation is a basic assumption. This law states that the sources of energy, principally solar or short-wave radiation absorbed by the surface and atmosphere, are balanced by the losses of energy, the emission of radiation to space.

The radiative equilibrium temperatures of the surface and atmosphere depend on the magnitude of the incoming solar energy and on the absorbing and emitting properties of the surface and atmosphere. The interplay of energy between the sun, Mars and space can be described by two energy balance equations, one for the surface and the other for the atmosphere. First, let us examine the important radiation components of the unit atmospheric column shown in Figure 1, and then develop the balance equations from these components.

Of the short-wave radiation incident at the top of the atmosphere (1), a small portion is absorbed by the atmosphere (2) before reaching the surface. A major portion of the solar radiation is absorbed by the surface (3) and the remaining energy is diffusely reflected back to the atmosphere (4) and to space (5). In this model, atmospheric scattering of energy is neglected and the atmosphere is assumed free of clouds. The planetary albedo of Mars is controlled mostly by the assumed surface reflectivity and to a lesser degree by atmospheric absorption.

In turn the surface emits long-wave radiation (6) back to the atmosphere (7) and to space (8). The atmosphere emits radiation to space directly (9) and emits radiation back to the surface. A major portion of this back radiation from the atmosphere is absorbed at the surface (10); a small portion is reflected back to the atmosphere (11) and to space (12).

In order to satisfy the conditions of radiative equilibrium, the gains and losses of energy at the top of the atmosphere, within the atmosphere and at the surface must all be equal; i.e., the net radiation is zero. The exchange of sensible heat at the surface-atmosphere interface and the storage of heat in the surface and atmosphere are neglected in this model. The equation which expresses the balance of energy gains and losses for the surface is given by

$$(1 - R_{s_o})F_{s_o} + \epsilon_o \epsilon_a (T_a)^4 \sigma T_a^4 = \epsilon_o \sigma T_o^4, \quad (1)$$

where R_{s_o} = the surface reflectivity to short-wave radiation,

F_{s_o} = the incident short-wave radiation at the surface,

ϵ_o = the surface emissivity to long-wave radiation,

$\epsilon_a(T_a)$ = the atmospheric emissivity to long-wave radiation, a function of the atmospheric temperature T_a ,

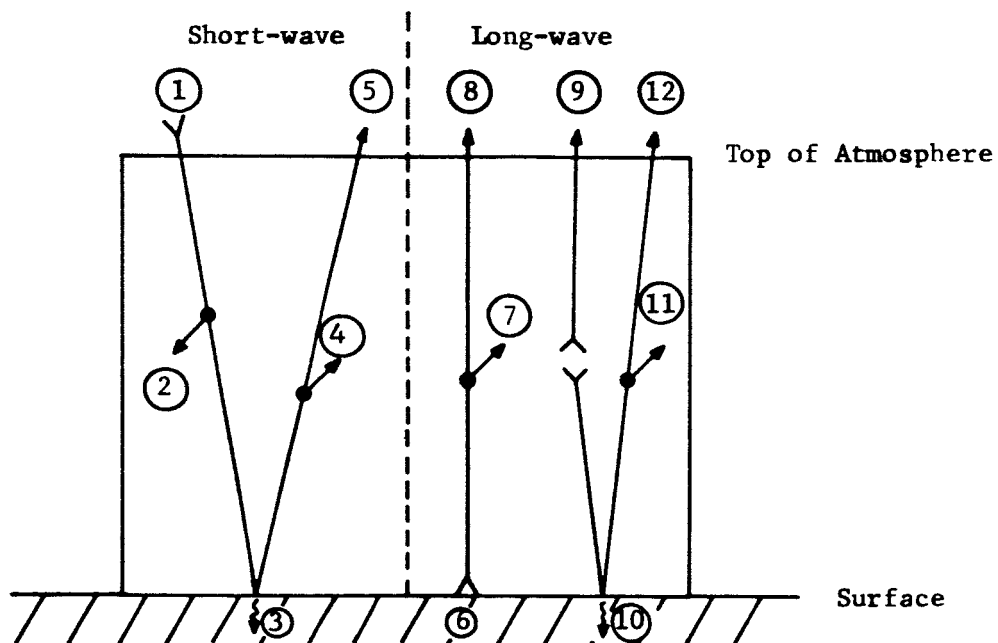


Figure 1. Radiation components of a unit atmospheric column.

σ = Stefan-Boltzmann's constant,
 T_o = the surface temperature in $^{\circ}\text{K}$.

The gains of energy to the left of Equation (1), respectively, are the absorbed short-wave radiation and the absorbed long-wave radiation emitted by the atmosphere. Both of these terms are balanced by the surface radiant energy loss.

A similar equation for the energy balance of the atmosphere is given by

$$F_{st} - F_{so} [1 - R_{so} (1 - e^{-1.66\tau})] + \epsilon_o \alpha_a (T_o) \sigma T_o^4 = [2 - (1 - \epsilon_o) \epsilon_a (T_a)] \epsilon_a (T_a) \sigma T_a^4 \quad (2)$$

where F_{st} = the insolation at the top of the atmosphere,
 τ = the optical thickness of the atmosphere to short-wave radiation,
 $e^{-1.66\tau}$ = the transmittance of the atmosphere to diffuse short-wave radiation, assuming $e^{-\tau}$ is the vertical beam transmittance of the atmosphere to direct short-wave radiation,
 $\alpha_a (T_o)$ = the absorptivity of the atmosphere to long-wave radiation from the surface.

The first two terms to the left of Equation (2) are the solar energy absorbed by the atmosphere, both the direct component and diffusely reflected component from the surface, and the third term is the absorbed long-wave radiation from the surface. These energy gains are balanced by the radiant energy loss by the atmosphere to the surface and space. The term $(1 - \epsilon_o)$ is the reflectivity of the surface to long-wave radiation from the atmosphere.

The solution for the mean atmospheric temperature, based on Equation (1) and (2), is

$$T_a = \left\{ \frac{F_{st} - F_{so} [1 - R_{so} (1 - e^{-1.66\tau})] + (1 - R_{so}) \alpha_a (T_o) F_{so}}{[2 - (1 - \epsilon_o) \epsilon_a (T_a) - \alpha_a (T_o) \epsilon_o] \epsilon_a (T_a) \sigma} \right\}^{\frac{1}{4}} \quad (3)$$

and the solution for the surface temperature using Equation (1) and the value of T_a from Equation (3) is

$$T_o = \left\{ \frac{(1 - R_{so}) F_{so} + \epsilon_o \epsilon_a (T_a) \sigma T_a^4}{\epsilon_o \sigma} \right\}^{\frac{1}{4}} \quad (4)$$

The calculation of atmospheric and surface temperatures using Equations (3) and (4) is complicated by the fact that the atmospheric absorptivity and

emissivity are dependent variables, and are functions, themselves, of the temperatures to be calculated. Thus, for example, the algebraic solution to determine the atmospheric temperature is not readily apparent for given values of solar energy input, and cannot be determined from a single calculation using the energy balance equations.

However, an exact solution to the equations can be found, using the method of successive approximations in the computer (trial and error method). The process of iteration is as follows: Values of atmospheric absorptivity and emissivity are assumed as an approximation to the exact values. Then the surface and atmospheric temperatures are computed using the energy balance equations. These computed temperatures establish new values of absorptivity and emissivity, which, in turn, yield better approximations to the equilibrium temperatures, etc. This iteration process converges rapidly to the exact solution of the energy balance equations. For example, the temperatures are accurate to within one degree of the exact solution after four or five iterations in the computer.

2.3 Method of Calculating Model Parameters

The principal input parameters needed for the calculations include the transmissivity of the atmosphere to a normal beam of solar radiation, $e^{-\tau}$, or the absorptivity, $1 - e^{-\tau}$, and the effective absorptivity and emissivity of the atmosphere to long-wave radiation, α_a and ϵ_a respectively. Of the gases that are assumed in the atmospheric compositions, nitrogen, carbon dioxide and water vapor, the latter two gases are optically active in both the short- and long-wave regions of the spectrum.

Atmospheric absorption of solar radiation by the near infrared bands of carbon dioxide and water vapor is computed using the method of Roach (1961) which is based on the experimental data of Howard, et al., (1955). Following the notation of Roach (1961), the amount of solar energy absorbed from a pressure level to the top of the atmosphere, E , is given by

$$E = \sum_i I_{oi} \cos \psi A_i \quad (5)$$

where I_{oi} is the intensity of solar radiation per wave number at the top of the atmosphere in the i^{th} absorption band, ψ is the solar zenith angle, A_i is the band area in wave numbers (cm^{-1}). Details of the method to calculate A_i are contained in Roach's article. The absorptivity of the atmosphere ($1 - e^{-\tau}$) to a normal beam of solar radiation $\psi = 0^\circ$, is given by

$$1 - e^{-\tau} = \frac{E}{S} = \frac{\sum_i I_{oi} A_i}{S} \quad , \quad (6)$$

where S is the total incident solar radiation, summed over all wave numbers. Therefore, the transmissivity of the atmosphere to normal solar radiation is

$$e^{-\tau} = 1 - \frac{\sum_i I_{oi} A_i}{S} \quad (7)$$

The method outlined by Elsasser and Culbertson (1960) is used to compute the effective absorptivity and emissivity of the atmosphere to long-wave radiation. The absorptivity to surface radiation is given by the expression

$$\alpha_a(T_o) = \frac{\int_0^{\infty} \alpha(\nu) I_o(\nu) d\nu}{\int_0^{\infty} I_o(\nu) d\nu} = \frac{\int_0^{\infty} \alpha(\nu) I_o(\nu) d\nu}{\sigma T_o^4} \quad (8)$$

where $\alpha(\nu)$ is the spectral absorptivity of the atmosphere at wave number ν at a given atmospheric temperature, and $I_o(\nu)$ is the emission intensity of the Planck function at the prevailing surface temperature T_o . In a similar manner the effective emissivity of the atmosphere is

$$\epsilon_a(T_a) = \frac{\int_0^{\infty} \epsilon(\nu) I_a(\nu) d\nu}{\int_0^{\infty} I_a(\nu) d\nu} = \frac{\int_0^{\infty} \epsilon(\nu) I_a(\nu) d\nu}{\sigma T_a^4} \quad (9)$$

where $I_a(\nu)$ is the emission intensity of the Planck function at the prevailing atmospheric temperature. The values of the spectral emissivity (absorptivity) are computed using Elsasser's method.

Both effective absorptivity and emissivity have a temperature dependence, owing to the change of the weighting distribution of the Planck function with wave number at different temperatures. This point will be discussed further in the next section, and then the calculated results of the annual mean temperature climate for different Martian atmospheres will follow.

2.4 Calculated Model Parameters for Different Martian Atmospheres

Four likely atmospheric compositions and surface pressures on Mars are considered in this study. Two of these atmospheres, listed in Table 1, follow from the radio occultation experiment on Mariner IV (Kliore, et al, 1965), and the second pair of atmospheres are based on the measurements of Kaplan, et al, (1964).

Table 1

Surface Pressure and Composition of
Possible Martian Atmospheres

Model No.	Surface Pressure (mb)	CO ₂ (mb)	N ₂ (mb)	^T CO ₂ (m atm)	Reference
1	5	5	0	68.6	Kliore (1965)
2	6	3	3	41.1	Kliore (1965)
3	10	6	4	82.2	Kaplan (1964)
4	25	4	19	54.8	Kaplan (1964)

Concerning the amount of water vapor on Mars, Spinrad pointed out at the recent Lunar and Planetary Conference in California that the amount of precipitable water vapor on Mars is variable with latitude. He suggested an average value of about $15 \mu \text{ H}_2\text{O cm}^{-2}$. Revised estimates presented by Dollfus at the same conference indicate values around $45 \mu \text{ H}_2\text{O cm}^{-2}$. Therefore, an average of these two figures was adopted for this study, $30 \mu \text{ H}_2\text{O cm}^{-2}$.

In the far infrared, three absorption bands at different wavelength regions of the spectrum affect the absorption and emission of radiation. These bands are the $15 \mu \text{ CO}_2$ band, the 6.3μ water vapor band and the rotational water vapor band. To get an idea of the relative strengths of these bands for the Martian atmospheres, the spectral emissivity of CO_2 and H_2O for Model No. 3 is plotted as a function of wave number, in Figure 2. These values are based on an atmospheric temperature of 190°K . The 15μ band is by far the strongest of the three bands owing to the large optical depth of CO_2 in the Martian atmosphere.

Spectral emissivity calculations for all models were computed at a variety of temperatures. These results indicate a slight variation of spectral emissivity in the wings of the CO_2 band for various optical depths. More of a variation in emissivity was noted with changing temperature. On the other hand, the centers and wings of the H_2O bands show a greater sensitivity to both pressure and temperature than is indicated by the CO_2 band.

When computing the effective emissivity of the atmosphere, the temperature dependence on the Planck function is greater than the variations of spectral emissivity with temperature. As the temperature increases, the wave number of maximum emission also increases in magnitude and shifts toward longer wave numbers. This change with temperature is shown qualitatively in Figure 2 by the dashed lines.

Computed variations of effective emissivity with temperature for carbon dioxide and water vapor, are shown in Figure 3. The effective emissivity for carbon dioxide, ϵ_{CO_2} , increases steadily with temperature, and then reaches a maximum value, corresponding to the shift of the Planck function maxima to wave numbers in the CO_2 absorption band. In the case of the effective emissivity for water vapor $\epsilon_{\text{H}_2\text{O}}$, the values increase and then decrease, corresponding to the shift of the Planck function maxima from wave numbers in the rotational band to higher wave numbers between the rotational and 6.3μ bands. The effective emissivity for the atmosphere, ϵ_a in Figure 3, is the sum of the curves for $\epsilon_{\text{H}_2\text{O}}$ and ϵ_{CO_2} , since there is no overlap of the absorption bands for the low atmospheric pressures found on Mars.

A curve similar to the one for $\epsilon_a(T_a)$ holds for the effective absorptivity, $\alpha_a(T_o)$, of the atmosphere to long-wave radiation from the surface. For a given temperature in Figure 3, α_a would equal to ϵ_a . It must be remembered, however, that α_a is a function of the surface temperature and ϵ_a is a function of the atmospheric temperature. Normally α_a is not equal to ϵ_a for a given calculation of the radiative heat budget.

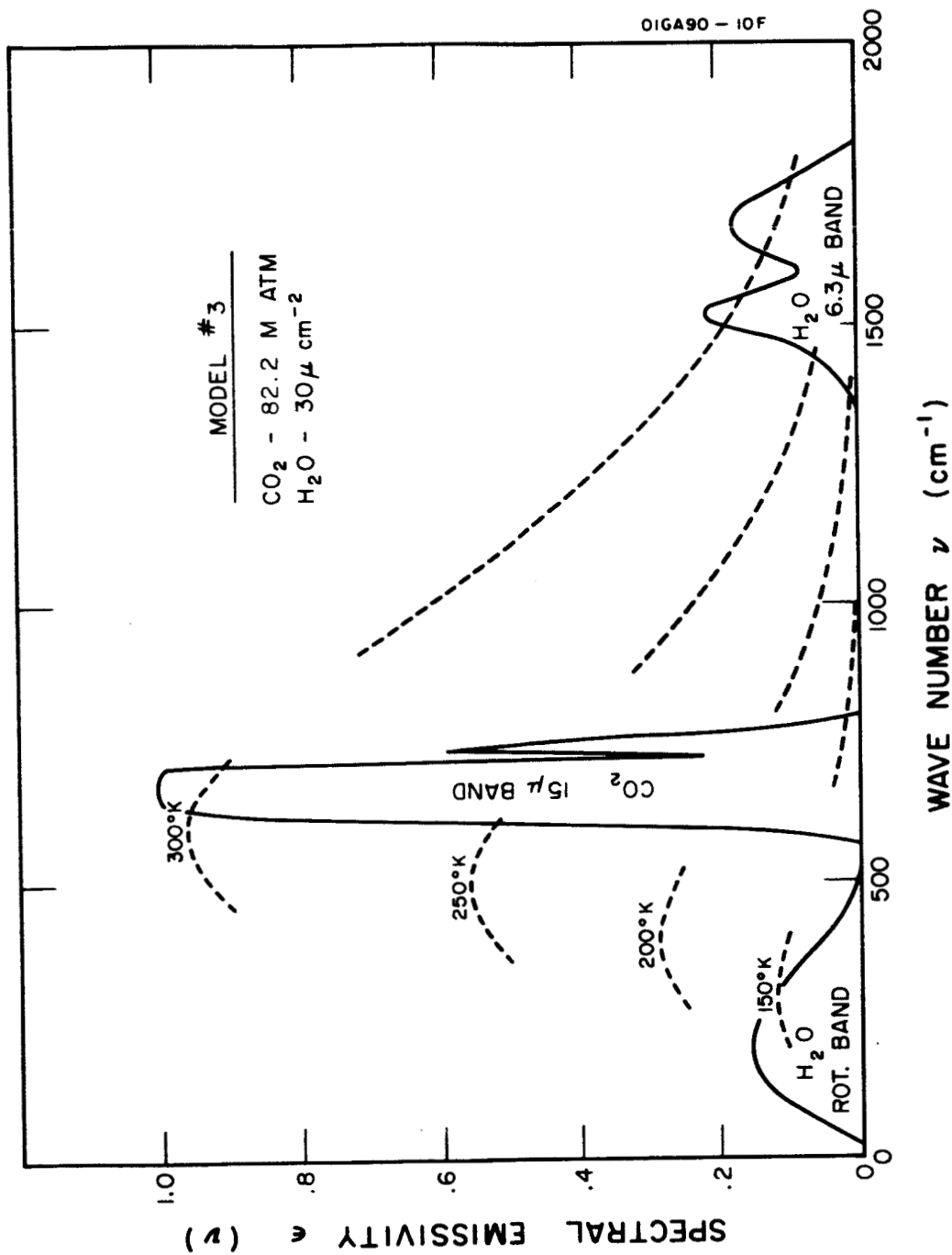


Figure 2. Variation of the spectral emissivity with wave number for an atmospheric temperature of 190°K. The relative emission intensities of the Planck function for different temperatures are indicated by the dashed lines.

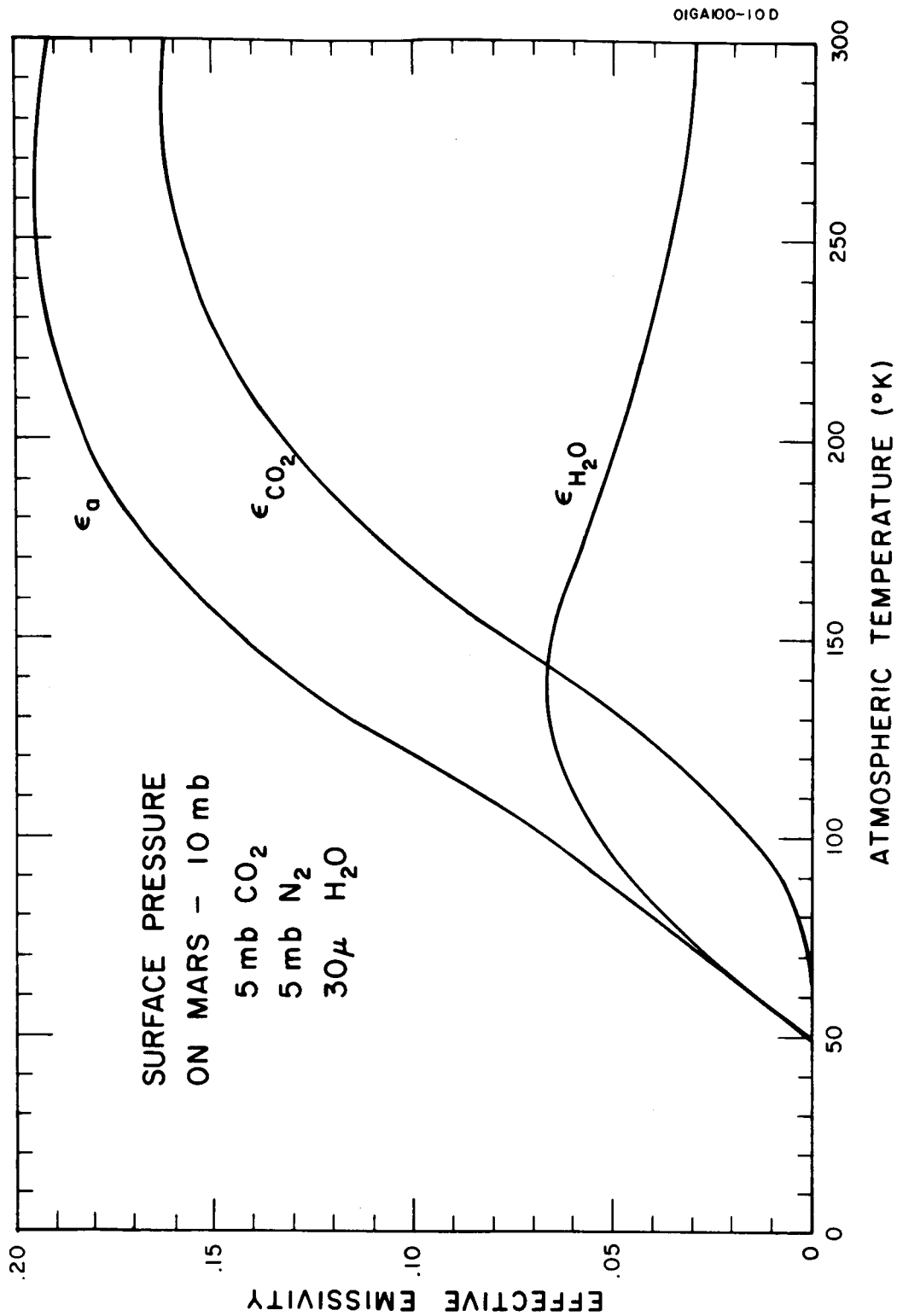


Figure 3. Variation of the effective emissivity of carbon dioxide, ϵ_{CO_2} , and water vapor, ϵ_{H_2O} , with atmospheric temperature. The sum of these curves is the effective emissivity for the atmosphere.

Calculated results of the short-wave absorptivities, the long-wave absorptivities (at 215°K) and the long-wave emissivities (at 190°K) are shown in Table 2. The table is further partitioned into the relative contributions of CO₂ and H₂O to each total value. As would be expected, the contribution by CO₂ is greater than that for H₂O, about three times greater in all categories of the table. There is a small variation in the CO₂ emissivity for the different models of ± 0.011 , whereas, a larger pressure dependence is noted in the H₂O emissivities of ± 0.016 . The temperature dependence of the emissivity due to the weighting of the Planck function mentioned earlier is evident when comparing the total absorptivity and emissivity columns for each model.

2.5 Average Surface and Atmospheric Temperatures

Calculation of the average surface and atmospheric temperatures on Mars is now possible using Equations (3) and (4). In addition to the parameters listed in Table 2, values of the surface reflectivity to short-wave radiation, the surface emissivity to long-wave radiation and the solar constant are required for the calculations.

De Vaucouleurs (1964) has made an extensive reappraisal of the planetary albedo of Mars. He suggests a value of 0.295 with an estimated probable error of ± 0.02 . A surface reflectivity of 0.310 in the equations is sufficient to account for this planetary albedo.

Measurements of the infrared emissivities of sandy surfaces by Buettner and Kern (1965) indicate that the emissivity of quartz sand varies between .914 and .928 depending on the grain size. Measurements of the spectral dependence of lunar emissivity by Murcray (1965) indicate values from 0.91 at 10.3μ to 0.98 at 8.5μ . Assuming that these surfaces are representative of the Martian surface, an emissivity of 0.925 was adopted for the calculations.

Based on a solar constant of $2.00 \text{ cal cm}^{-2} \text{ min}^{-1}$ (Johnson, 1954) and de Vaucouleurs' albedo, the average rate of absorbed radiation on Mars is $0.152 \text{ cal cm}^{-2} \text{ min}^{-1}$ which corresponds to an effective temperature of 207.7°K for the planet in the absence of an atmosphere. Since the atmosphere on Mars acts as a greenhouse, the average surface temperature will be somewhat warmer than 207.7°K, and the average atmospheric temperature will be somewhat cooler than this temperature.

The results of the surface and atmospheric temperature calculations are presented in Table 3. Inspection of these values indicates that the temperature climate on Mars is rather insensitive to the choice of atmospheric composition and surface pressure. The surface temperature range is $\pm 0.7^\circ\text{K}$ and the atmospheric temperature range is $\pm 1.5^\circ\text{K}$. Ohring and Mariano's (1965) calculations of the average temperature structure of the Martian atmosphere for a variety of models indicate the same insensitiveness of atmospheric temperature to the choice of composition and surface pressure.

Table 2

Computed Absorptivities and Emissivities for Each Martian Atmosphere

Model No.	Short-Wave		Long-Wave		Long-Wave				
	Absorptivity		Absorptivity (215°K)		Emissivity (190°K)				
	H ₂ O	CO ₂	CO ₂	H ₂ O	CO ₂	H ₂ O			
	Total		Total		Total				
1	.00167	.00731	.00898	.134	.033	.167	.116	.042	.158
2	.00176	.00540	.00716	.129	.036	.165	.113	.046	.159
3	.00209	.00910	.01119	.146	.042	.188	.126	.053	.179
4	.00275	.01000	.01275	.152	.063	.215	.131	.076	.207

Table 3

Average Surface and Atmospheric
Temperatures on Mars

Model No.	Surface Temperature	Atmospheric Temperature
1	214.7°K	187.7°K
2	214.7	185.3
3	215.3	188.3
4	216.0	188.2

Based on this evidence, a single atmospheric composition and pressure, representative of the models discussed in this report, is suitable for the study of the seasonal climatology of Mars. A surface pressure of 10 mb consisting of 5 mb CO₂ and 5 mb N₂ seems to be a reasonable choice. The resulting optical depth of CO₂ would be 68.6 m atm; the 10 mb surface pressure would produce a broadening of the H₂O bands which is representative of the H₂O absorptivities and emissivities listed in Table 2.

2.6 Seasonal Climatology Results

Calculation of the latitudinal distribution of surface and atmospheric temperatures was carried out at ten-day intervals for the entire Martian year. These results give some indication of the variations of temperatures within a seasonal period. In addition to the temperature calculations at ten-day intervals, the average input of solar energy at the top of the atmosphere and at the surface was computed for each season and for the annual mean. From these results it is possible to compute representative, seasonal average surface and atmospheric temperatures as well as the mean annual temperatures.

The graphs in Figure 4 show the latitudinal variation of the average daily insolation on Mars at the top of the atmosphere for the different seasons and for the annual mean. Units are in cal cm⁻² day⁻¹ where a day represents one Martian day, 1477 minutes. In these calculations, the seasons represent time periods of the Martian year which are centered about the equinoxes and solstices. Thus, Summer is the warm season, Winter is the cold season, and Spring and Fall represent the transitional seasons between the extremes. Such a division of seasons has more meaning in a meteorological and climological sense than the astronomical division of the seasons which is taken to be the periods between the solstices and equinoxes.

Curves for the variation of insolation at the surface of Mars are similar to those shown in Figure 4 except that they are slightly reduced in magnitude. On the average for the annual mean, about 2.0 percent of the solar radiation is absorbed by the atmosphere before reaching the surface. This absorption varies with latitude, being about 1.7 percent at the equator and 3.8 percent at the poles. For long slant paths through the atmosphere, the absorption of solar radiation by the atmosphere can be as much as 13 percent of the incident energy.

The graphs in Figures 5, 6, and 7 summarize the calculated results of the seasonal climatology on Mars using the radiative equilibrium model. The contrasting seasons of Winter and Summer are compared in Figure 5, the latitudinal variation of surface and atmospheric temperatures for the Spring and Fall seasons are shown in Figure 6, and the summary of the mean annual temperatures is indicated in Figure 7.

Each set of curves for the seasons has a discontinuity at latitudes ranging from 20° to 60°. These discontinuities represent the equatorward extension of the polar ice caps and are based on the dew point temperature

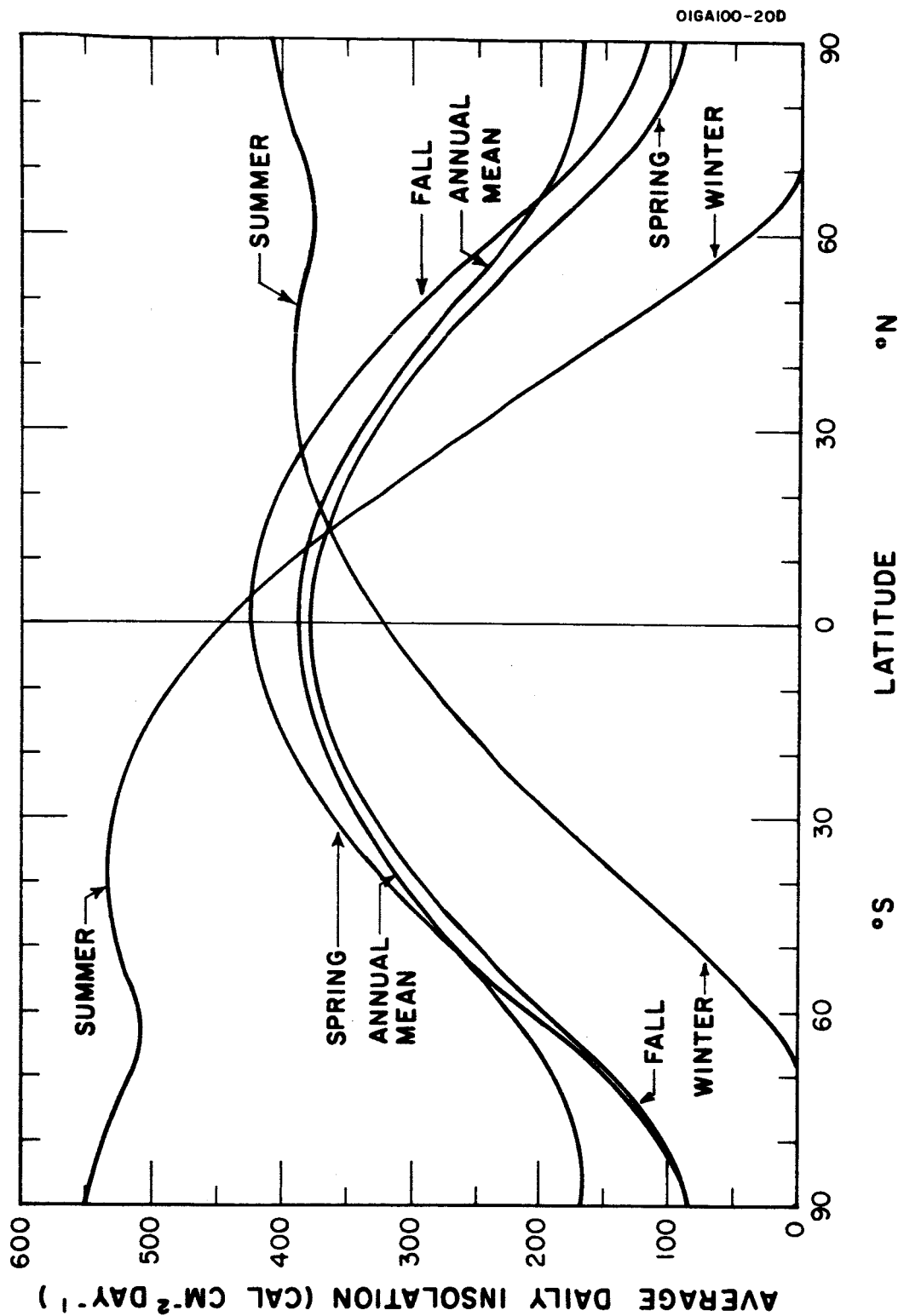


Figure 4. The latitudinal variation of the average daily insolation on Mars at the top of the atmosphere. The spring and fall seasons and the summer and winter seasons represent periods of the Martian year which are centered about the equinoxes and solstices, respectively. A solar constant of $2.00 \text{ cal cm}^{-2} \text{ min}^{-1}$ is assumed in the calculations.

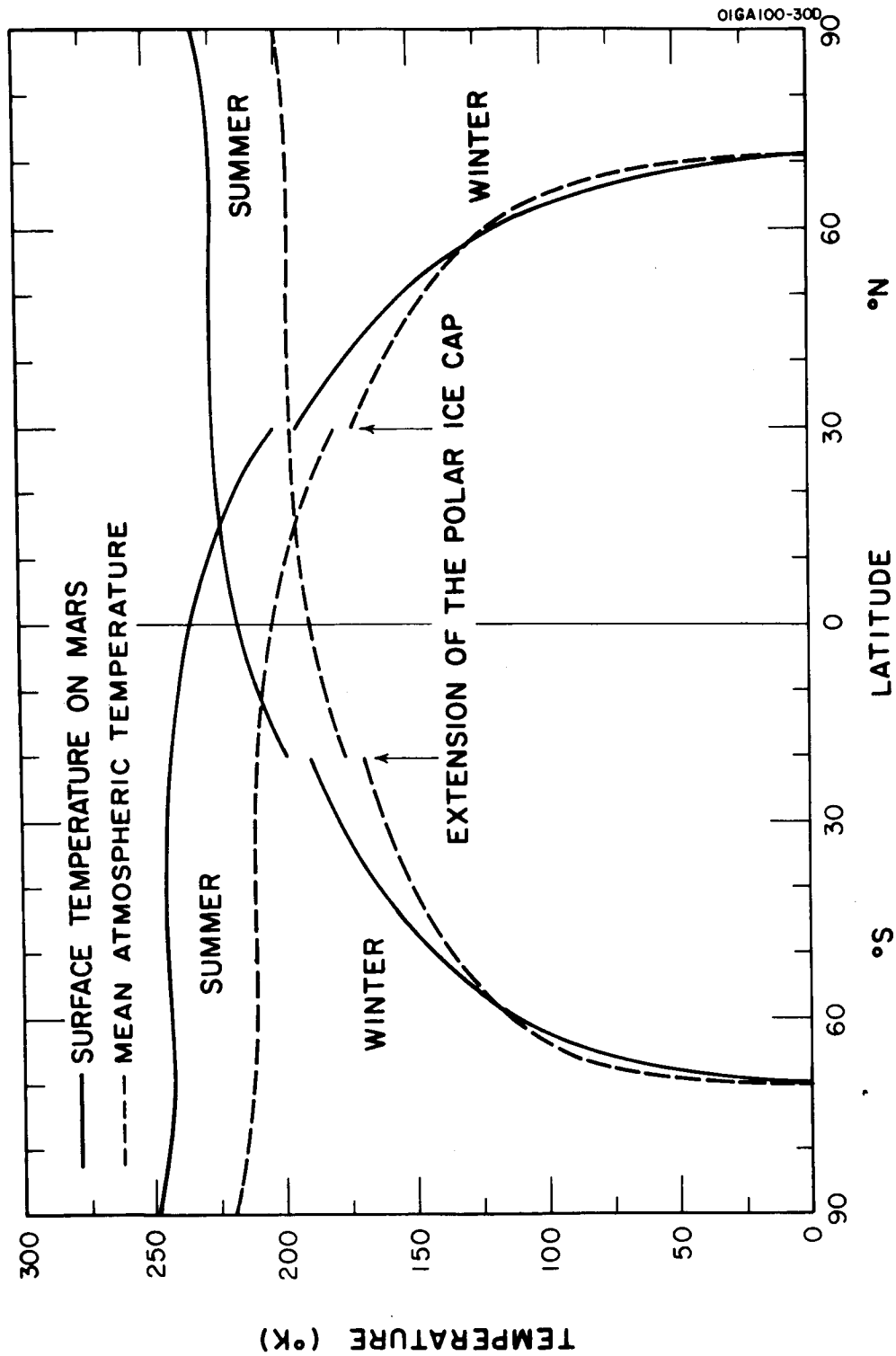


Figure 5. Latitudinal variation of the average surface and atmospheric temperatures on Mars for the summer and winter seasons. The equatorward extension of the polar ice cap is indicated by the discontinuity in the lines.

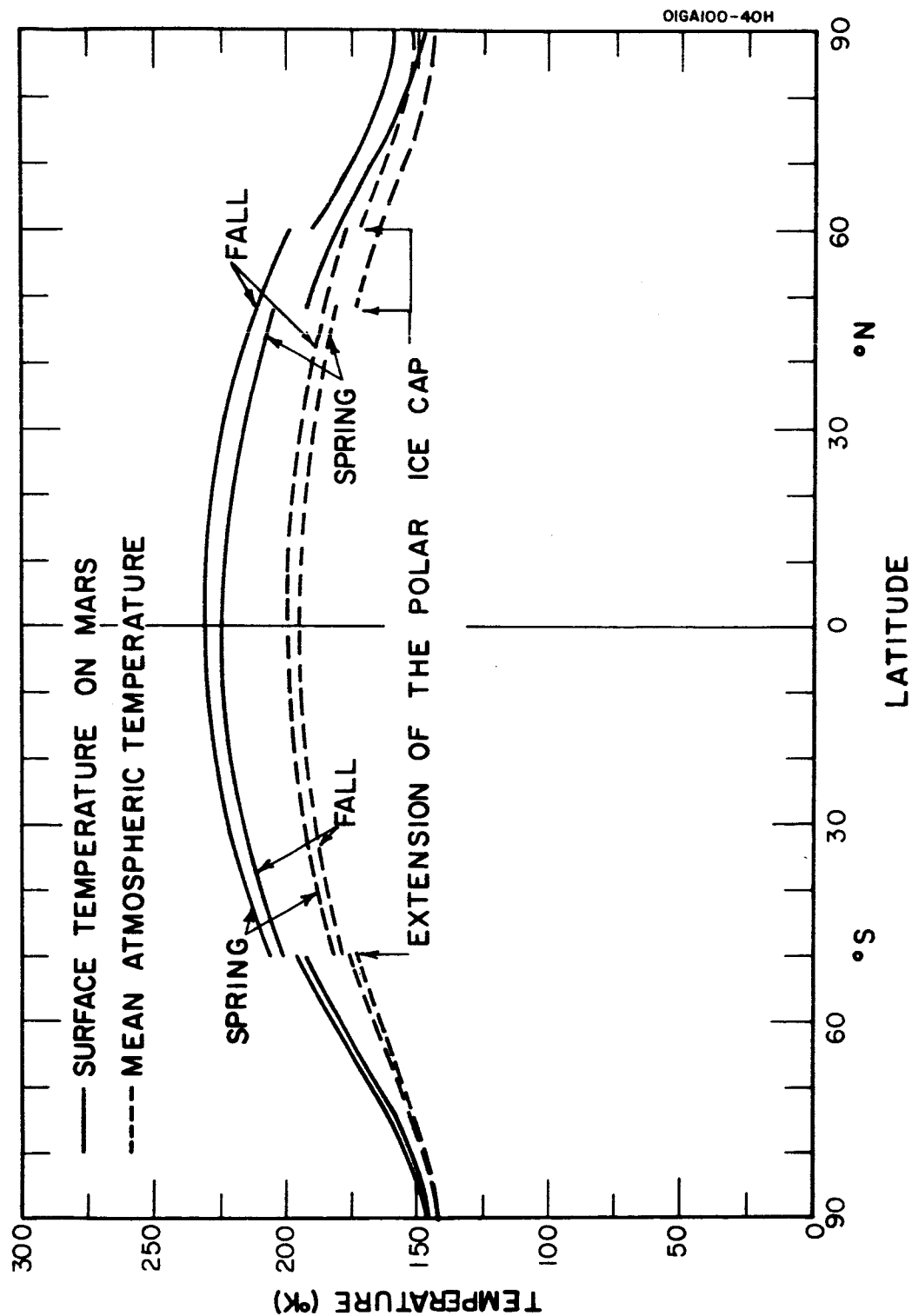


Figure 6. Latitudinal variation of the average surface and atmospheric temperatures on Mars for the spring and fall seasons. The equatorward extension of the polar ice cap is indicated by the discontinuity of the lines.

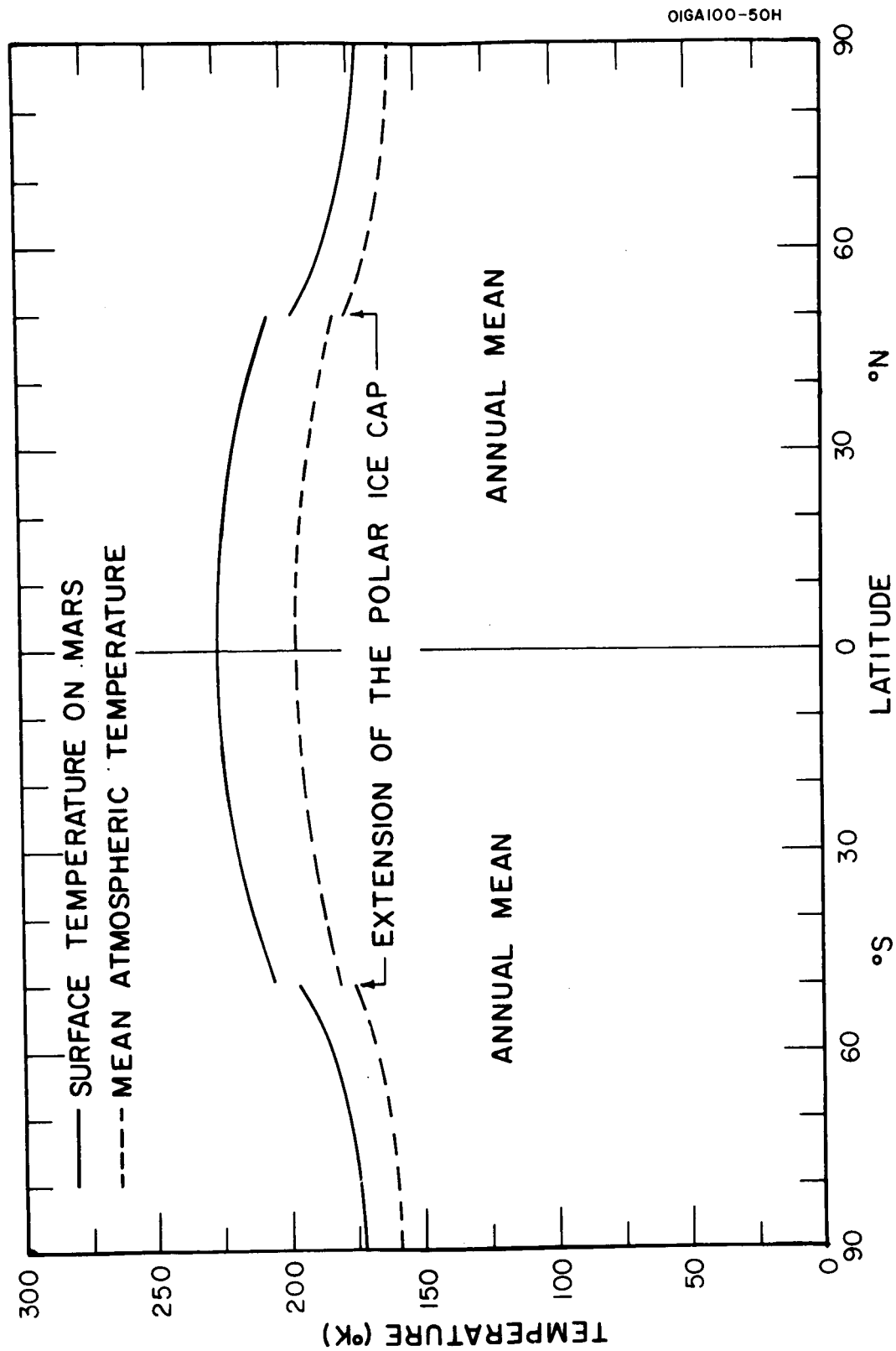


Figure 7. Latitudinal variation of the average surface and atmospheric temperatures on Mars for the annual mean. The discontinuity in the lines indicates the equatorward extension of the polar ice cap.

of the atmosphere at the surface. Assuming that the 30 microns of precipitable water vapor in the atmosphere are evenly mixed, the dew point at the surface for a 10 mb surface pressure is 202°K . Thus, in the calculations, if the computed surface temperature was below 202°K , it was assumed that the ice cap had formed and that the albedo of the surface increased from 31 percent to 45 percent, the approximate albedo of dirty snow. As a result, the computed values of surface and atmospheric temperatures decrease with the albedo increase, thus, producing a discontinuity in the temperature profiles.

Some of the salient features of the seasonal climatology on Mars are evident from an analysis of the temperature profiles. In Figure 5, it is evident that the summer poles in both hemispheres have the highest average surface temperature, the south pole temperature (248°K) being somewhat warmer than the north pole temperature (230°K). The mean atmospheric temperatures during a summer run about 30°C colder than the computed surface temperatures, and the pole to equator temperature difference in each hemisphere is quite small during summer, about 12 to 14°C .

In contrast to the summer seasons, the winter seasons show a marked decrease in temperatures at latitudes poleward of the equator. The curves in Figure 5 indicate that the difference between the surface and atmospheric temperatures decreases with increasing latitude, and, at latitudes greater than 58° , the mean atmospheric temperature is larger than the surface temperature. Such a temperature configuration as this suggests a strong temperature inversion at the surface which is indeed the case on Earth at high latitudes during winter. Two factors contribute to these warmer atmospheric temperatures at high latitudes: 1) greater absorption of solar radiation by the atmosphere relative to surface absorption because of the long slant path through the atmosphere, and 2) the effective emissivity of the atmosphere decreases with temperature.

In Figure 6, the Spring and Fall seasons in both hemispheres indicate similar temperature profiles. As in the case of the Summer seasons, the temperature difference between the surface and atmosphere is about 30°C at the equator. This difference decreases with increasing latitude, diminishing to about 6.5°C at the poles. The temperature profiles indicating Spring in the southern hemisphere and Fall in the northern hemisphere are somewhat warmer than the profiles for the opposing seasons, because the planet is closer to the sun at this time.

The profiles in Figure 7 indicate the mean annual temperature climate on Mars. Probably the most pronounced feature of these results is the symmetry of temperatures about the equatorial region, the northern hemisphere being slightly warmer due to the greater amount of insolation received there in the annual mean. Surface and atmospheric temperatures at the equator are 226.1°K and 196.3°K , respectively, and decrease to about 173.3°K and 160.5°K at the poles.

The effect of the atmospheric transport of heat on the temperature climate, computed from the radiative equilibrium model, would be a decrease in the

temperature gradients with latitude, especially the atmospheric temperature gradient. This effect would be quite evident during the winter seasons at high latitudes during the polar night. When using the radiative equilibrium model, the computed temperatures are zero because there is no solar input of energy. With heat transport into these latitudes, the temperature will increase to between 125°K and 150°K , depending on the latitude. In the case of the Summer seasons, the effect of heat transport will have hardly any effect on the pole to equator temperature gradient and will cause only a small lowering of the temperature magnitudes. The effect produced by heat transport for the Spring and Fall seasons will be somewhat larger than would be expected for the Summer season.

REFERENCES

- Arking, A., 1963: Non-grey planetary atmospheres. Mem. Soc. R. Sci., Liege, 5, 180-189.
- Buettner, K.J.K., and C.D. Kern, 1965: The determination of infrared emissivities of terrestrial surfaces. J. Geophys. Res., 70, No. 6, 1329-1337.
- Coblentz, W.W., and Lampland, C.O., 1923: Measurements of planetary radiation. Lowell Obs. Bull., No. 85.
- de Vaucouleurs, G., 1964: Geometric and photometric parameters of the terrestrial planets. Icarus, 3, 187-235.
- Gifford, F., 1956: The surface-temperature climate of Mars. Astrophys. J., 123, 154-161.
- Goody, R.M., 1957: The atmosphere of Mars. Weather, 12, 3-15.
- Howard, J.N., D.L. Burch, and D. Williams, 1955: Near infrared transmission through synthetic atmospheres. G.R.P. 40, ASTIA AD-87679.
- Johnson, F.S., 1954: The solar constant. J. Meteor., 11, No. 1, 431-439.
- Kaplan, L.D., G. Munch, and H. Spinrad, 1964: An analysis of the spectrum of Mars. Astrophys. J., 139, 1-15.
- Kliore, A., D.L. Cain, G.S. Levy, Von R. Eshleman, G. Fjeldbo, and F.D. Drake, 1965: Occultation experiment: Results of the first direct measurement of Mars' atmosphere and ionosphere. Science, 49, 1243-1248.
- Milankovitch, M., 1920: Theorie mathematique des phenomenes thermiques produits par la radiation solaire. Paris sec. 65, 'Le Climat de la Planete Mars.'
- Murcray, F.H., 1965: The spectral dependence of lunar emissivity. J. Geophys. Res., 70, No. 19, 4959-4962.
- Ohring, G., 1963: A theoretical estimate of the average vertical temperature distribution in the Martian atmosphere. Icarus, 1, 328-333.
- Prabhakara, C., and J.S. Hogan, 1965: Ozone and carbon dioxide heating in the Martian atmosphere. J. Atmos. Sci., 22, 2, 97-109.
- Roach, G.T., 1961: The absorption of solar radiation by water vapor and carbon dioxide in a cloudless atmosphere. Quart. J. Roy. Meteor. Soc., 87, 364-373.
- Sinton, W.M., and J. Strong, 1960: Radiometric observations of Mars. Astrophys. J., 131, 459-469.

3. WATER VAPOR MIXING RATIOS NEAR THE CLOUD-TOPS OF VENUS

George Ohring

3.1 Introduction

From an analysis of the near infrared reflection spectrum of the Cytherian clouds, Bottema, et al (1964) have concluded that the clouds are composed of ice crystals. Arguments against ice (or water) clouds on Venus have been given by Sagan and Kellogg (1963) and, more recently, by Chamberlain (1965). These arguments are based upon a comparison of the water vapor mixing ratio derived from the observations of water vapor amounts above the Cytherian clouds and the required saturation mixing ratio for condensation at the observed cloud-top temperatures. Such a comparison indicates that the water vapor mixing ratios are much below those required for condensation. However, the computations by Sagan and Kellogg, and Chamberlain, are based upon the assumption that the water vapor mixing ratio is constant with altitude above the clouds. This is not necessarily the case. In the Earth's atmosphere, for example, the water vapor mixing ratio generally decreases with altitude. In this paper, we investigate whether condensation can occur at the cloud-tops, if the water vapor mixing ratio decreases with altitude at rates comparable to those in the Earth's atmosphere.

3.2 Discussion

The water vapor mixing ratio is defined as the ratio of the density of water vapor to the density of the dry atmosphere containing the water vapor. However, to a high degree of approximation, it can be represented as

$$w = \frac{\rho_v}{\rho} \quad (1)$$

where w is the mixing ratio, ρ_v is the water vapor density, and ρ is the total density of the atmosphere. Spectroscopic observations yield the total amount of water vapor above a given reflecting level, which is equivalent to

$$\int_z^{\infty} \rho_v dz ,$$

with units of g cm^{-2} . The results of several such observations are shown in Table 1. It may be noted that Bottema, et al (1965) give two different values based upon two different reflecting levels. These reflecting levels are based upon the estimates of the cloud-top pressure given by Sagan and Kellogg (1963):

TABLE 1

OBSERVATIONS OF WATER VAPOR ON VENUS

Investigators	$\int \rho_v dz$ (g/cm ²)	Presumed Reflecting Level (mb)
Spinrad (1962)	$< 7 \times 10^{-3}$	8,000
Dollfus (1963)	1×10^{-2}	90
		600
Bottema, et al (1965)	1.23×10^{-2}	90
	2.9×10^{-3}	600

90 mb to 600 mb. Spinrad (1962) gives only an upper limit to the possible amount of water vapor. Furthermore, Spinrad's observation refers to the total amount of water vapor above a level deep in the atmosphere. Dollfus' (1963) estimate of $1 \times 10^{-2} \text{ g cm}^{-2}$ is based upon an assumed reflecting level somewhat lower than 1 atmosphere. For purposes of these computations, we have assigned values of 90 mb and 600 mb to associate with Dollfus' observations. There is some uncertainty in the reflecting levels assumed by Dollfus and by Bottema, et al; their observations may refer to reflecting levels somewhat deeper in the atmosphere than the level of the cloud-top.

If it is assumed that the water mixing ratio is constant with altitude, its value can be obtained as follows. From the definition of mixing ratio

$$\rho_v = w\rho \quad (2)$$

Integrating both sides with respect to height, and using the hydrostatic equation, we have

$$\int_z^\infty \rho_v dz = w \int_z^\infty \rho dz = \frac{w}{g} p_z \quad (3)$$

where p_z is the pressure at the reflecting level, and g is the gravitational acceleration. The mixing ratio can then be written as

$$w = \int_z^\infty \rho_v dz / (p_z/g) \quad (4)$$

In Figures 1 and 2, the results of such computations for the data of Bottema, et al (1965) and Dollfus (1963) are shown with the label $k = 0$. Spinrad's own estimate of the maximum water vapor mixing ratio — 10^{-5} — is also shown.

These values are to be compared with the saturation mixing ratio at the temperature of the cloud-top. The saturation mixing ratio is

$$w_s = \frac{m_v}{m} \left(\frac{e_s}{p} \right)_z \quad (5)$$

where m_v/m is the ratio of the molecular weight of water vapor to the molecular weight of the Cytherian atmosphere, and e_s is the saturation vapor pressure, which depends upon the temperature of the cloud-top. If we assume that the molecular weight of the Cytherian atmosphere is equal to that of nitrogen, $m_v/m = 0.64$. The 8-13 μ thermal emission observations of Sinton and Strong (1960) suggest a cloud-top temperature of about 235K. Chamberlain (1965), after applying a correction for scattering, suggests an upper limit of about

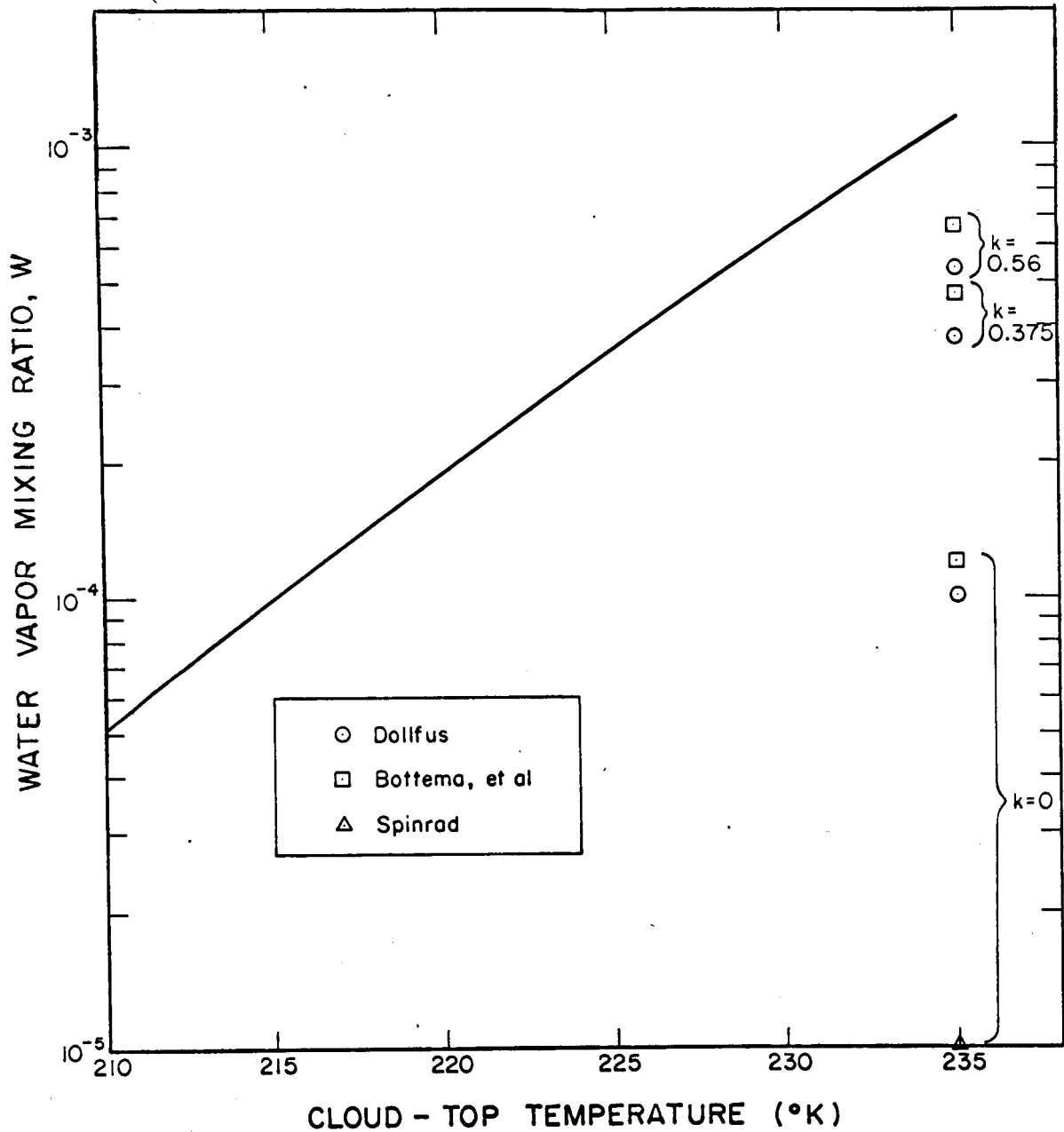


Figure 1. Water vapor mixing ratios at the Cytherian cloud-top for a cloud-top pressure of 90 mb. Solid line represents mixing ratios required for saturation; points represent mixing ratios computed from observations.

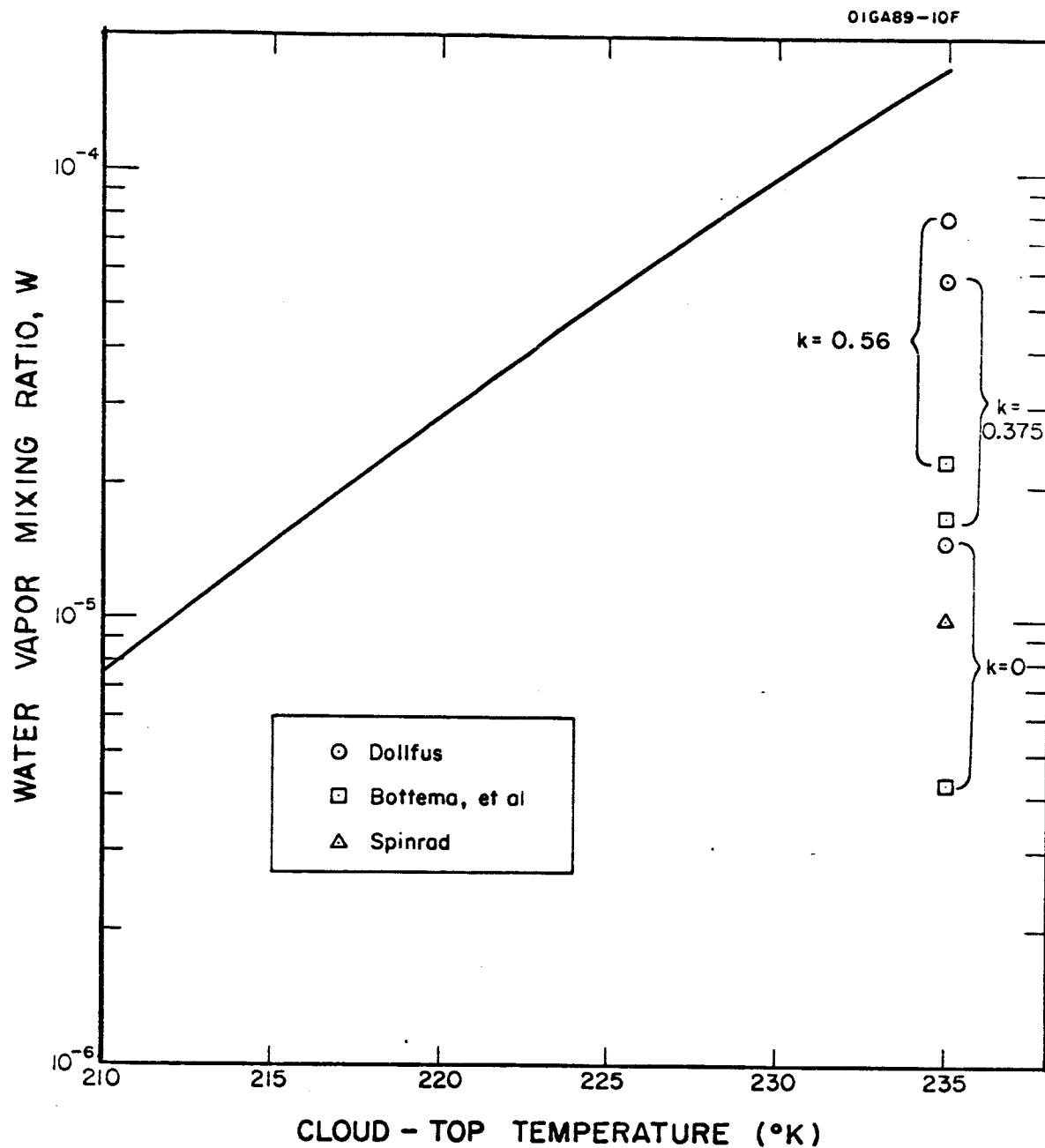


Figure 2. Water vapor mixing ratios at the Cytherian cloud-top for a cloud-top pressure of 600 mb. Solid line represents mixing ratios required for saturation; points represent mixing ratios computed from observations.

255 K for the cloud-top temperature. The 8-14 μ thermal emission observations of Murray, et al (1963) indicate a cloud-top temperature of 208K, but they state that their observed temperatures are systematically too low because of uncertain telescope transmission losses. Pollack and Sagan (1965) have evaluated in detail several models of the atmosphere and clouds in an attempt to explain the observed limb darkening of Venus in the 8-13 μ interval. They suggest a convective cloud model, in which the limb darkening is caused by absorption and scattering within the clouds, as the most likely explanation of the observed limb darkening. For reasonable values of the parameters in this model, and based upon an overall disc temperature at 8-13 μ as measured by Sinton and Strong (1960), cloud-top temperatures of about 210K are obtained. Thus, as the above discussion indicates, there is, at present, some uncertainty in the value of the cloud-top temperature. The lines in Figures 1 and 2 show the variation of saturation mixing ratio with temperatures as the cloud-top temperature varies from 210K to 235K. The constant mixing ratios ($k = 0$) are clearly at least an order of magnitude less than the saturation mixing ratio at a cloud-top temperature of 235K, and also less than the saturation values at cloud-top temperatures as low as 215K. On the basis of similar computations, Sagan and Kellogg (1964) and Chamberlain (1965) have questioned the aqueous nature of the Cytherian clouds.

Gutnick (1962) has analyzed the variation of water vapor mixing ratio with altitude at middle latitudes in the Earth's atmosphere. In the troposphere, the average mixing ratio decreases logarithmically with altitude. Such a decrease can be represented by

$$\frac{d \ln w}{dz} = -k \quad (6)$$

Gutnick's data indicate that the average value of k is about 0.375 km^{-1} between the surface and 7 km, and about 0.56 km^{-1} between 7 and 14 km.

If we assume similar variations of mixing ratio with altitude above the Cytherian clouds, keeping the total water vapor amount consistent with the observations, what mixing ratios would we obtain at the cloud-top? We have

$$w = w_0 e^{-kz} \quad (7)$$

for the variation of mixing ratio above the clouds. (For constant mixing ratio, $k = 0$.) The variation of water vapor density with altitude can then be written as

$$\rho_v = \rho \left(\frac{\rho_v}{\rho} \right)_0 e^{-kz} \quad (8)$$

where the subscript zero refers to the cloud-top. The variation of atmospheric density with altitude is

$$\rho = \rho_0 e^{-z/H} \quad (9)$$

where H is the scale height. For a nitrogen atmosphere with a temperature of 235K and $g = 880 \text{ cm/sec}^{-2}$, $H = 7.9 \text{ km}$. Substituting Equation (9) into Equation (8), we have

$$\rho_v = (\rho_v)_0 e^{-(0.127+k)z} \quad (10)$$

The integral of Equation (10) with respect to height must be equal to the observed total amount of water vapor above the cloud,

$$\int_0^{\infty} \rho_v dz = (\rho_v)_0 \int_0^{\infty} e^{-(0.127+k)z} dz \quad (11)$$

Integrating the right hand side of Equation (11) and solving for $(\rho_v)_0$, we find

$$(\rho_v)_0 = (0.127 + k) \int_0^{\infty} \rho_v dz \quad (12)$$

The mixing ratio at the cloud top can then be obtained from $(\rho_v/\rho)_0$, where ρ_0 is computed from

$$\rho_0 = \frac{mp}{R^* T} \quad (13)$$

where p and T are the pressure (90 mb and 600 mb) and approximate temperature (235K) at the cloud top, and R^* is the universal gas constant. Cloud-top mixing ratios computed in this manner for the data of Bottema, et al (1965) and Dollfus (1963) are shown in Figures 1 and 2, where they are labeled $k = 0.375$ and $k = 0.56$. Spinrad's data are not treated in this way since if one were to assume an exponential decrease of water vapor mixing ratio above his presumed reflecting level of 8,000 mb, the computed water vapor mixing ratios at 90 mb or 600 mb would be less than that computed for the assumption of constant mixing ratio, and, hence, would depart further from the required saturation mixing ratio. Thus, no matter what assumption is made about the variation of water vapor with altitude, Spinrad's data appear to be incompatible with an aqueous cloud.

It is apparent from Figures 1 and 2 that these mixing ratios are much closer than the constant mixing ratios to the required saturation mixing ratios at a cloud-top temperature of 235K. And if the actual cloud-top temperature were just 5-10C lower, saturation would actually occur for some of these cases. Thus, at least for the observations of Bottema, et al (1965) and Dollfus (1963), the observed water vapor amounts are compatible with an ice crystal cloud if the cloud-top temperature is 225K to 230K or less, and the water vapor mixing ratio decreases with altitude at a rate comparable to that in the Earth's upper troposphere.

3.3 Conclusions

There is no reason to believe that the assumption of a constant mixing ratio above the Cytherian cloud is better than the assumption of a logarithmic decrease. In fact, a better case can be made for the assumption of a logarithmic decrease since, if the clouds are composed of water substance, the variation of mixing ratio with altitude might be similar to that observed above terrestrial clouds. A reasonable estimate of such a variation is the average value of the upper atmospheric variation of mixing ratio in the Earth's atmosphere. As indicated above, this value leads, under certain conditions, to cloud-top mixing ratios compatible with the presence of clouds composed of water substance. Thus, we may conclude that compatibility between the observed water vapor amounts and the presence of water clouds on Venus can be achieved under certain conditions. Or, put another way, the observed water vapor amounts, at the present state of our knowledge, are not incompatible with the presence of water clouds on Venus.

REFERENCES

- Bottema, M., W. Plummer, J. Strong, and R. Zander, 1964: Composition of the clouds of Venus, Astrophys. J., 139, 1021-1022.
- Bottema, M., et al., 1965: A quantitative measurement of water vapor in the atmosphere of Venus, Annales D'Astrophysique, 28, 225-228.
- Chamberlain, J.W., 1965: The atmosphere of Venus near her cloud tops. Astrophys. J., 141, 1184-1205.
- Dollfus, A., 1963: Observation of water vapor on the planet Venus, Compt. Rend., 256, 3250-3253.
- Gutnick, M., 1962: Mean annual mid-latitude moisture profiles to 31 km. Air Force Surveys in Geophysics, 147, AFCRL, 30 pp.
- Murray, B.C., et al., 1963: Infrared photometric mapping of Venus through the 8- to 14-micron atmospheric window. J. Geophys. Res. 68, 4812-4818.
- Pollack, J.B., and C. Sagan, 1965: The infrared limb darkening of Venus. J. Geophys. Res. 70, 4403-4426.
- Sagan, C., and W. W. Kellogg, 1963: The terrestrial planets. Ann. Rev. Astron. Astrophys. 1, 235-266.
- Spinrad, H., 1962: A search for water vapor and trace constituents in the Venus atmosphere. Icarus, 1, 266-270.

4. INTERHEMISPHERIC TRANSPORT OF WATER VAPOR AND THE MARTIAN ICE CAPS

George Ohring and Joseph Mariano

4.1 Introduction

One of the fundamental problems of the meteorology of Mars concerns its ice caps. The amount of water vapor in the Martian atmosphere is about 10^{-3} g cm⁻² (Kaplan et al, 1964). The thickness of the ice caps is of the order of 1 cm (de Vaucouleurs, 1961). During the course of the Martian year, as one polar ice cap forms, the other sublimates and completely disappears. The amount of water vapor in the atmosphere, even if it were all to condense, could not account for the formation of the ice caps. Thus, it has been suggested that, as one ice cap melts, the water vapor released into the atmosphere is transported to the opposite pole, where it condenses. At any one time, then, most of the Martian water vapor is located in the polar caps. During each Martian year, there is an atmospheric shuttling of water vapor from one pole to the other.

There are two possible atmospheric mechanisms that might accomplish the required transport: a mean meridional velocity and large-scale atmospheric diffusion. The rate of transport from one pole to the other is probably greatest during the equinoctial seasons, when one cap is melting and the other is forming. During these seasons, the Martian temperatures are probably highest at the equator and lowest at the poles. With such a temperature distribution, a meridional circulation system would be characterized by equatorward motion at the surface and poleward motion aloft. The mean meridional velocity pattern required to explain the ice cap formation is characterized by a surface flow from the melting polar cap to the forming polar cap. Obviously, the required flow is not compatible with the probable flow pattern during the equinoctial seasons. As the solstice approaches, the summer pole heats up and may become the hottest point on the planet. A meridional circulation system at this time would be characterized by flow from summer pole to the winter pole at upper levels and the reverse near the surface. Again, the required flow — from summer to winter pole near the surface — is not compatible with the probable Martian flow pattern. Thus, a mean meridional velocity does not appear to be a satisfactory explanation of the inter-hemispheric transport of water vapor. In this paper we investigate whether the other possible explanation — large-scale atmospheric diffusion — is reasonable, and attempt to determine the values of the large-scale diffusion coefficients required to accomplish the required transports of water vapor.

In the Earth's atmosphere, large-scale latitudinal transports of heat, momentum, and trace substances, such as water vapor, are accomplished by large-scale eddy diffusion processes. There are indications that within an individual hemisphere thorough mixing of a trace constituent can occur over

time periods of the order of months (Junge, 1962). Interhemispheric mixing times, on the other hand, have variously been estimated to be from 0.9 years to 4 years (Junge, 1963). For the Martian ice cap cycle, an interhemispheric mixing time of the order of one Earth year is required, since a complete ice cap cycle is completed in about two Earth years. Such a mixing time does not seem improbable when compared with the above values for Earth.

In the following discussion, we describe a simple global diffusion model, in which water vapor is released into the atmosphere by the melting of a north polar ice cap on Mars. With reasonable values for a large-scale diffusion coefficient, we calculate the latitudinal variation of water vapor as a function of time to see how rapidly the water vapor can proceed from one pole to the other.

4.2 Discussion

It is assumed that the transport of water vapor is entirely due to large-scale meridional diffusion, with a diffusion coefficient, K , independent of latitude and time. The concentration of water vapor, $q(\mu, t)$ (grams/cm²), where $\mu = \sin \theta$, θ being the angle of latitude, and the sources and sinks, $Q(\mu, t)$ (grams/cm²/sec), are related by the following equation:

$$\frac{\partial q}{\partial t} = \frac{K}{a^2} \frac{\partial}{\partial \mu} \left[(1 - \mu^2) \frac{\partial q}{\partial \mu} \right] + Q, \quad (1)$$

where a is the radius of the planet.

Since the set of Legendre polynomials, $P_n(\mu)$ satisfies the equation

$$\frac{\partial}{\partial \mu} \left[(1 - \mu^2) \frac{\partial P_n(\mu)}{\partial \mu} \right] = -n(n+1) P_n(\mu), \quad (2)$$

$q(\mu, t)$, and $Q(\mu, t)$ are expanded in Legendre polynomials:

$$q(\mu, t) = \sum_{n=0}^{\infty} q_n(t) P_n(\mu) \quad (3)$$

$$Q(\mu, t) = \sum_{n=0}^{\infty} Q_n(t) P_n(\mu), \quad (4)$$

where the coefficients, q_n and Q_n , are functions of time. Taking the Laplace transform of $q(\mu, t)$, $Q(\mu, t)$, and $\partial q / \partial t$, we get

$$\bar{q}(\mu, p) = \sum_{n=0}^{\infty} \bar{q}_n(p) P_n(\mu) \quad (5)$$

$$\bar{Q}(\mu, p) = \sum_{n=0}^{\infty} \bar{Q}_n(p) P_n(\mu) \quad (6)$$

$$\mathcal{L} \left\{ \frac{\partial q}{\partial t} \right\} = \sum_{n=0}^{\infty} [p \bar{q}_n(p) - q_n(0)] P_n(\mu) \quad (7)$$

In (7) the set, $\{q_n(0)\}$, are the coefficients in the expansion of $q(\mu, 0)$, the initial concentration of water vapor. Inserting Equations (5), (6), and (7) into Equation (1), we get

$$\sum_{n=0}^{\infty} [p \bar{q}_n(p) - q_n(0) + (n)(n+1) \frac{K}{a^2} \bar{q}_n(p) - \bar{Q}_n(p)] P_n(\mu) = 0 \quad (8)$$

which gives the following equation relating \bar{Q}_n and \bar{q}_n :

$$\bar{q}_n(p) = \frac{[\bar{Q}_n(p) + q_n(0)]}{p + \frac{K}{a^2} (n)(n+1)} \quad (9)$$

To obtain the inverse transform, we use the convolution theorem,

$$\mathcal{L} \left\{ \int_0^t f(x) g(t-x) dx \right\} = \bar{f}(p) \cdot \bar{g}(p) \quad (10)$$

where $\bar{f}(p) = \bar{Q}_n(p)$, and

$$\bar{g}(p) = \frac{1}{p + \frac{K}{a^2} (n)(n+1)} .$$

Thus, the equation relating the source coefficients and the concentration coefficients is:

$$q_n(t) = \int_0^t Q_n(x) \exp \left[-\frac{K}{a^2} (n)(n+1)(t-x) \right] dx + q_n(0) \exp \left[-\frac{K}{a^2} (n)(n+1)t \right] . \quad (11)$$

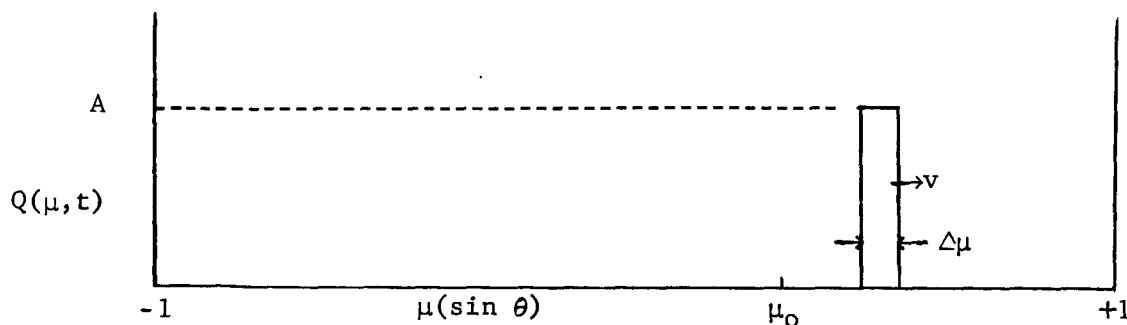
We assume a north polar cap one centimeter thick extending from 60° latitude to the north pole. Initially, there is no water vapor in the atmosphere; therefore, the second term on the right hand side of Equation (11) is zero. The polar cap sublimates at a constant rate per unit area for 12 terrestrial months ($\sim 1/2$ Martian year). Sublimation occurs only along the perimeter of the cap, and, thus, the cap recedes toward the pole and disappears at the end of the twelfth month.

As the total amount of water released by the source function is equal to the total amount of water in the cap prior to sublimation, the following equation must hold,

$$\int_0^T \int_0^{4\pi a^2} Q(\mu, t) dS dt = h \int_{\text{Area of the ice cap}} dS , \quad (12)$$

where T is the time when sublimation ends, h (1 cm) is the thickness of the ice cap, and dS is a differential unit of area equal to $2\pi a^2 d\mu$.

The source function consists of a step function of width $\Delta\mu$ and height A (see sketch below).



At time $t = 0$, the left hand side of the above step function is at μ_0 , where $\mu_0 = \sin 60^\circ$; the velocity of recession of the cap is such that at the end of 12 terrestrial months the source has crossed the boundary $\mu = 1$, $v = 4.5 \times 10^{-9} \text{ sec}^{-1}$; the width of the source, $\Delta\mu$, was chosen to be as small as practical, since sublimation is taking place only at the perimeter of the ice cap — the computer program constructed for this model allowed a value, $\Delta\mu = .03$; and the amplitude, A , is obtained from Equation (12).

The left hand side of Equation (12) is

$$\int_0^T \int_0^{4\pi a^2} Q(\mu, t) dS dt = \left(A \Delta\mu T_1 + \int_{T_1}^T A(1 - \mu_0 - vt) dt \right) 2\pi a^2 \quad (13)$$

where $\Delta\mu = .03$,
 $T_1 = 24.439 \times 10^6 \text{ sec}$ (the instant the source function reaches the N.P.)
 $T = 31.104 \times 10^6 \text{ sec}$ (the instant the source function passes the N.P.)
 $\mu_0 = .866$,
 $v = 4.50 \times 10^{-9} \text{ sec}^{-1}$.

And, with an ice cap thickness of 1 cm ($h = 1$), we obtain from Equations (12) and (13) the amplitude of the source function

$$A = .168 \times 10^{-6} \text{ grams/cm}^2 \text{ sec} .$$

This source function $Q(\mu, t)$ is expanded in Legendre polynomials to obtain the coefficients $Q_n(t)$ for Equation (4). These coefficients are then inserted into Equation (11) to obtain $q_n(t)$. The coefficients $q_n(t)$ are then inserted into Equation (3) to obtain $q(\mu, t)$, the concentration of water vapor as a function of latitude and time. Computations were performed for several different values of K , the large scale eddy diffusion coefficient.

4.3 Results

Figures 1 to 4 show the distribution of water vapor concentration as a function of latitude and time for large scale eddy diffusion coefficients ranging from $10^9 \text{ cm}^2 \text{ sec}^{-1}$ to $10^{11} \text{ cm}^2 \text{ sec}^{-1}$. The north pole cap starts sublimating at time $t = 0$ and completely disappears at time $t = 12$ months. Times are in terrestrial months, so that 12 months corresponds to approximately 1/2 Martian year. To explain the formation of the south polar cap by large scale meridional diffusion of water vapor from the sublimating north polar cap to

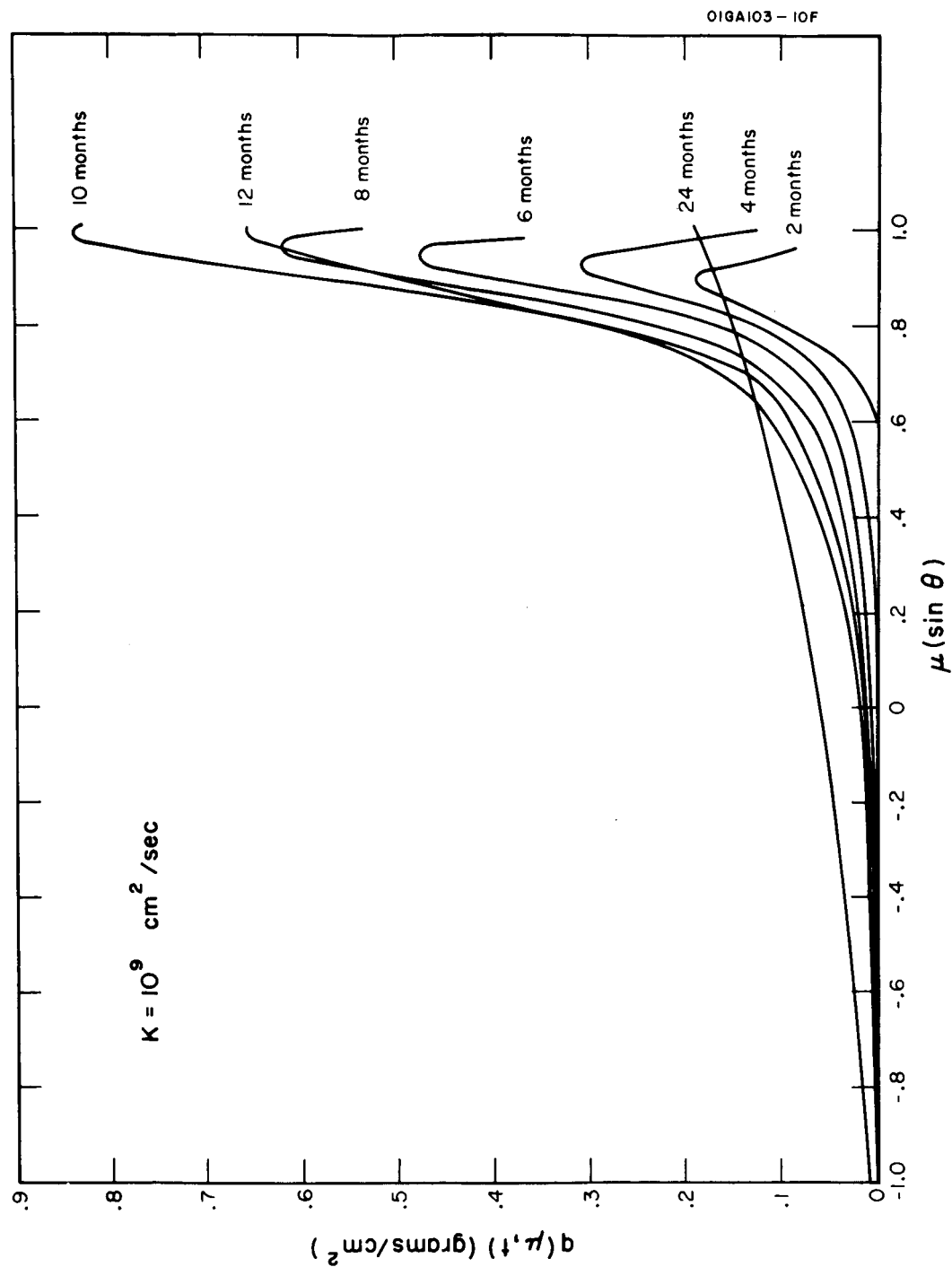


Figure 1. Latitudinal distributions of water vapor for various times after the Martian north polar cap starts to sublimate. $K = 10^9 \text{ cm}^2 \text{ sec}^{-1}$. (All times are in terrestrial months; 12 terrestrial months $\approx 1/2$ Martian year.)

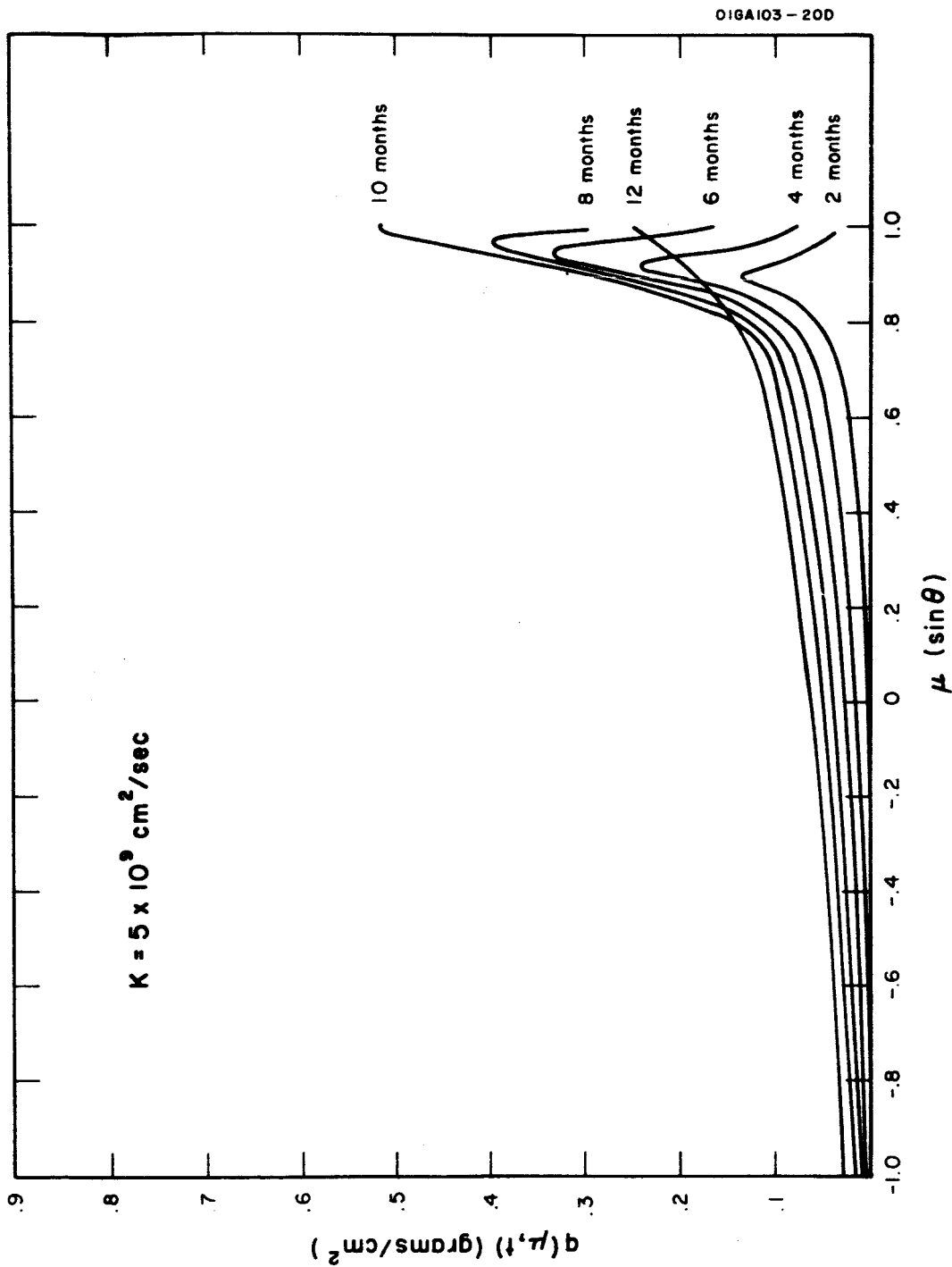


Figure 2. Latitudinal distributions of water vapor for various times after the Martian north polar cap starts to sublimate. $K = 5 \times 10^9 \text{ cm}^2 \text{ sec}^{-1}$. (All times are in terrestrial months; 12 terrestrial months $\approx 1/2$ Martian year.)

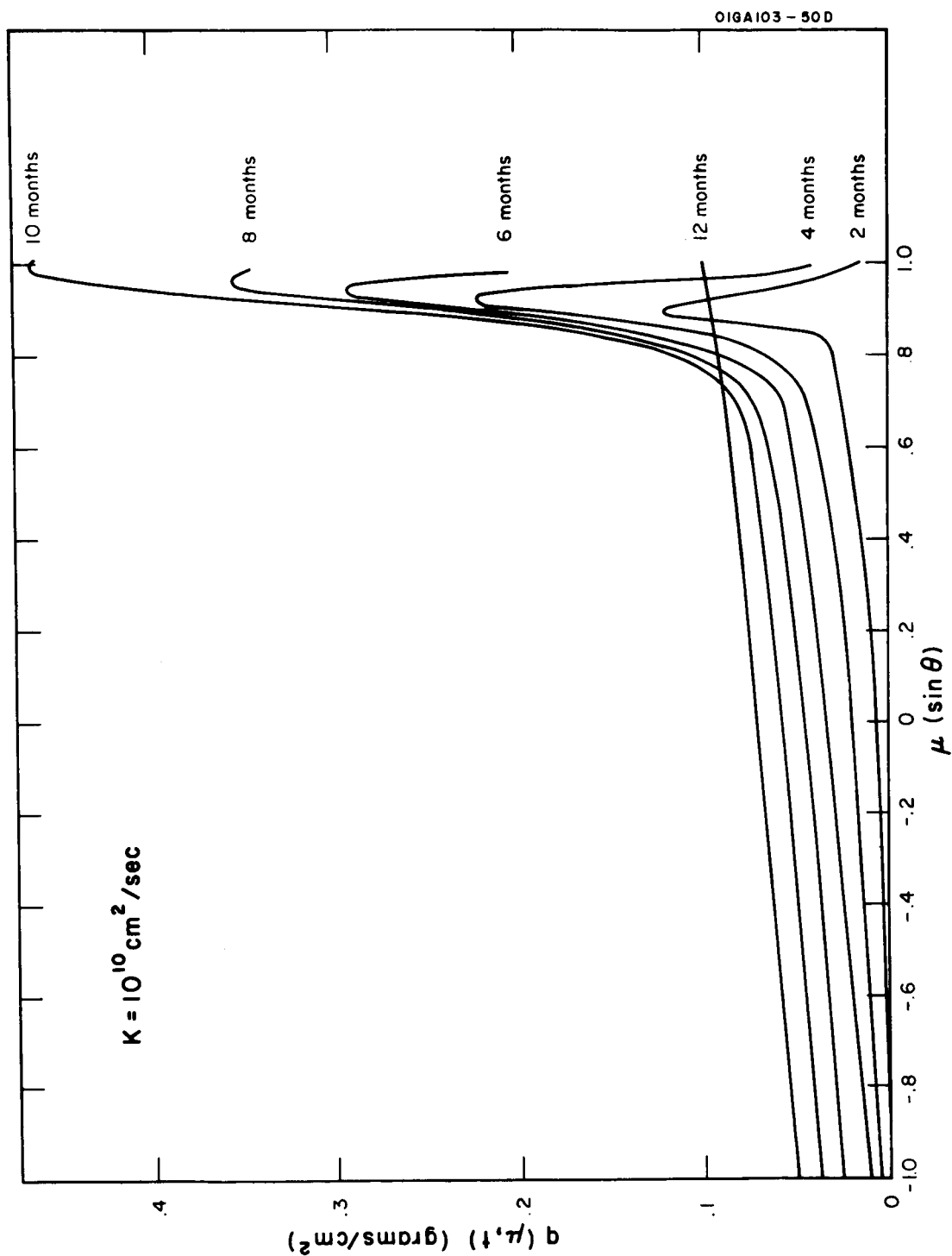


Figure 3. Latitudinal distributions of water vapor for various times after the Martian north polar cap starts to sublimate. $K = 10^{10} \text{ cm}^2 \text{ sec}^{-1}$. (All times are in terrestrial months; 12 terrestrial months $\approx 1/2$ Martian year.)

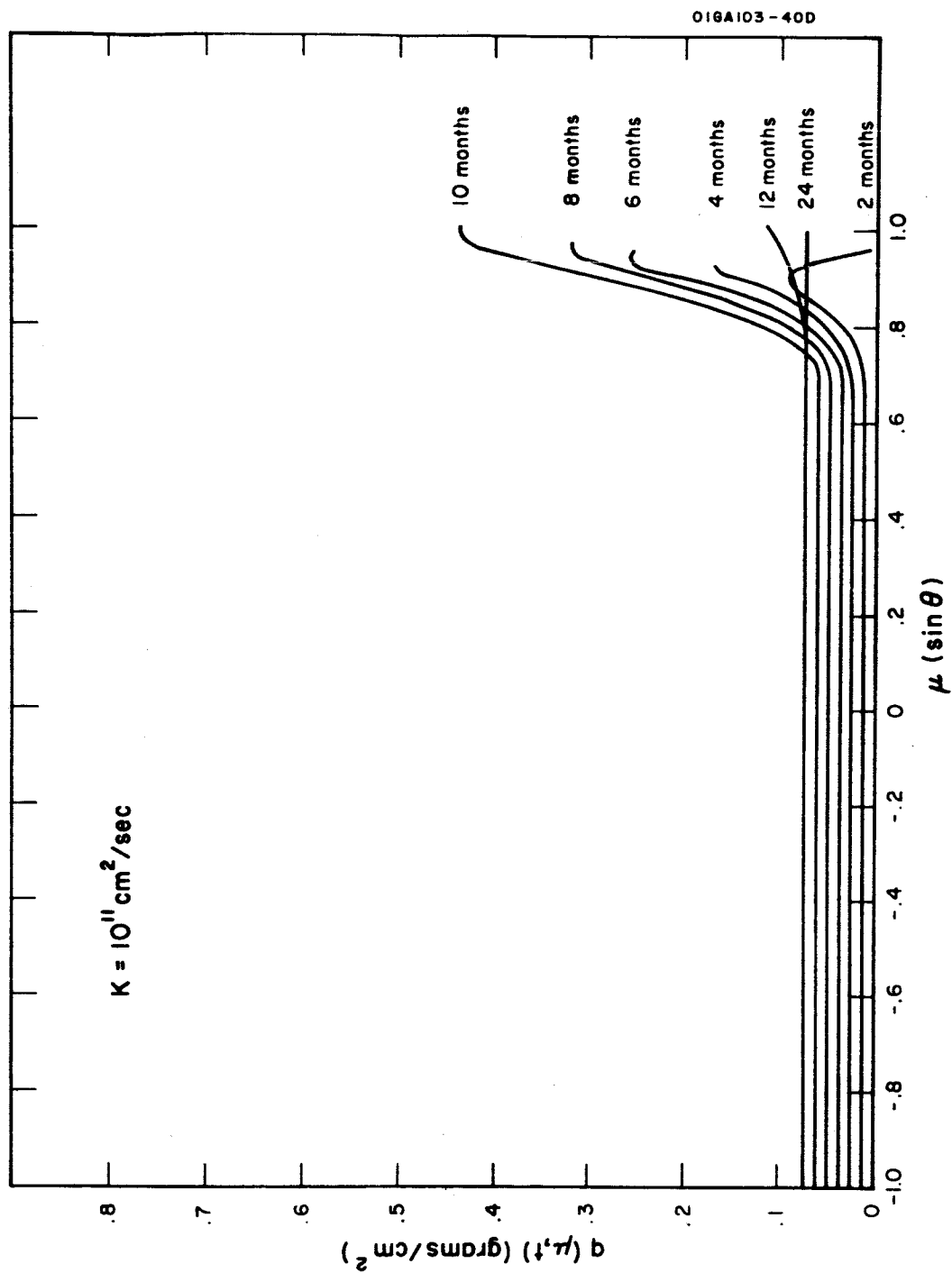


Figure 4. Latitudinal distribution of water vapor for various times after the Martian north polar cap starts to sublimate. $K = 10^{11} \text{ cm}^2 \text{ sec}^{-1}$. (All times are in terrestrial months; 12 terrestrial months $\approx 1/2$ Martian year.)

the opposite hemisphere, all or most of the water vapor released by the north polar cap must be transported to the south polar regions during a period of 1/2 Martian year — since the south polar cap is observed to grow to maximum size during the same period of time that the north polar cap is sublimating.

Since, in the present model, there is no sink for water vapor in the south polar regions, the maximum amount of water vapor that can be transported by the diffusion mechanism to the southern hemisphere is 1/2 of the total water in the north polar cap. At the time when this limit is reached, the concentration of water vapor would be constant with latitude over the entire planet at a value of about 0.07 g cm^{-2} . This equilibrium condition is reached sometime after 12 months for each of the values of large scale diffusion coefficient — occurring earliest for the highest diffusion coefficient. For example, with $K = 10^{11} \text{ cm}^2 \text{ sec}^{-1}$, the distribution of water vapor with latitude is already almost constant at $t = 12$ months, whereas, with $K = 10^9 \text{ cm}^2 \text{ sec}^{-1}$, most of the water vapor is still in the northern hemisphere at $t = 24$ months. With the knowledge that, for this model, equilibrium is attained at 0.07 g cm^{-2} , we can examine how close the south pole water vapor concentrations are to equilibrium at $t = 12$ months for the various diffusion coefficients. For $K = 10^9 \text{ cm}^2 \text{ sec}^{-1}$ and $K = 5 \times 10^9 \text{ cm}^2 \text{ sec}^{-1}$, the south pole concentrations are so far from equilibrium that they can probably be considered too small to produce the required interhemispheric transport of water vapor. For $K = 10^{10}$ and $K = 10^{11}$, the south pole water vapor concentrations at $t = 12$ months are very close to equilibrium. Therefore, this model suggests that the minimum value of the diffusion coefficient required to accomplish the interhemispheric transport of water vapor is about $10^{10} \text{ cm}^2 \text{ sec}^{-1}$.

Figure 5 shows the fractional amount of water vapor in the southern hemisphere as a function of time for the various diffusion coefficients. This fraction is the total amount of water vapor in the southern hemisphere divided by the total amount of water vapor originally contained in the north polar ice cap. As indicated above, this fraction has a maximum value of 0.5 for the present diffusion model. At $t = 12$ months 98 percent of the maximum value is attained for $K = 10^{11} \text{ cm}^2 \text{ sec}^{-1}$; almost 90 percent of the maximum value is attained for $K = 10^{10} \text{ cm}^2 \text{ sec}^{-1}$; about 60 percent of the maximum value is attained for $K = 5 \times 10^9 \text{ cm}^2 \text{ sec}^{-1}$; and only 10 percent of the maximum value is attained for $K = 10^9 \text{ cm}^2 \text{ sec}^{-1}$. These results again suggest that a diffusion coefficient of at least $10^{10} \text{ cm}^2 \text{ sec}^{-1}$ is required to accomplish the necessary interhemispheric water vapor transport.

It is of interest to compare the speeds of meridional propagation of isopleths of water vapor concentrations with the observed meridional speed of propagation of the Martian wave of darkening that proceeds toward the equator as the polar cap sublimates. The wave of darkening has an average speed of 30 km/day (Dollfus, 1961). The velocities of the isopleths are computed as the isopleths are travelling from the north pole to the equator. The computed meridional velocities of these water vapor isopleths as a function of time for the different diffusion coefficients are shown in Tables 1 to 3. For $K = 10^9 \text{ cm}^2 \text{ sec}^{-1}$, the average meridional speed of propagation of an isopleth; \bar{V} is 6 km/day; for $K = 5 \times 10^9 \text{ cm}^2 \text{ sec}^{-1}$, \bar{V} is 22 km/day; for $K = 10^{10} \text{ cm}^2 \text{ sec}^{-1}$, \bar{V} is 33 km/day; and,

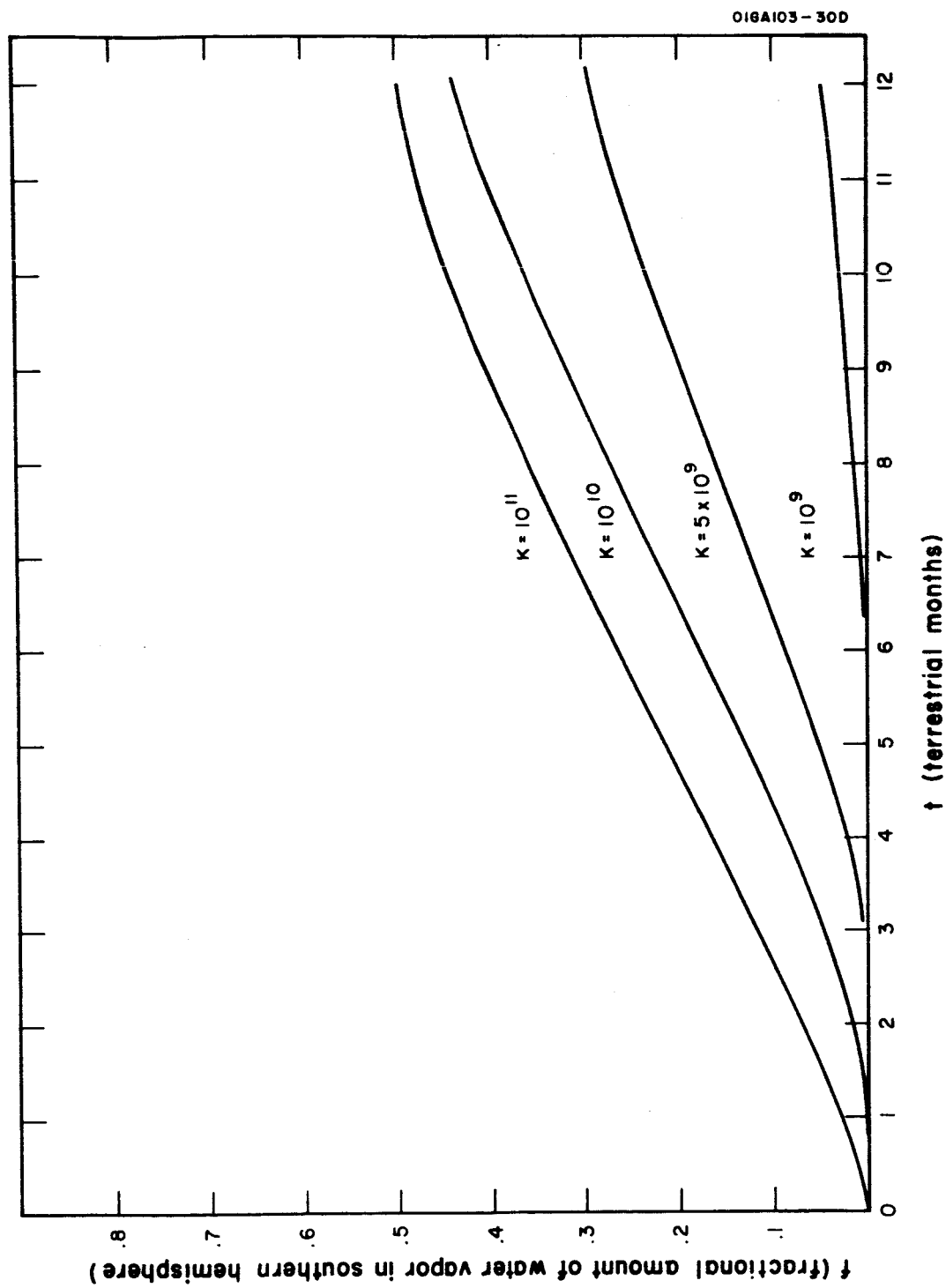


Figure 5. Fractional amount of water vapor in the Martian Southern Hemisphere as a function of time for different large scale eddy diffusion coefficients.

TABLE 1

Meridional velocity (km/day) of water vapor isopleths
(grams/cm²) for 3, 5, 7, 9, and 11 terrestrial months.
 $K = 10^9 \text{ cm}^2 \text{ sec.}$

t (Terrestrial Months)	Water Vapor Isopleths				
	q(grams/cm ²)				
	.02	.04	.06	.08	.10
3	11	4	4	4	3
5	12	6	5	5	3
7	7	7	11	11	13
9	7	6	4	4	5
11	4	4	3	3	4
\bar{V}	8	5	5	5	5

$$\bar{V} = 6 \text{ km/day.}$$

TABLE 2

Meridional velocity (km/day) of water vapor isopleths
(grams/cm²) for 3, 5, 7, and 9 terrestrial months.

$$K = 5 \times 10^9 \text{ cm}^2/\text{sec}.$$

t (Terrestrial Months)	Water Vapor Isopleths q(grams/cm ²)				
	.01	.02	.03	.04	.05
3	35	24	19	15	10
5		21	18	16	15
7					13
9					13
\bar{V}	35	22	19	15	13

$$\bar{V} = 22 \text{ km/day}.$$

TABLE 3

Meridional velocity (km/day) of water vapor isopleths
(grams/cm²) for 3, 5, 7, and 9 terrestrial months.

$$K = 10^{10} \text{ cm}^2/\text{sec}.$$

t (Terrestrial Months)	Water Vapor Isopleths q (grams/cm ²)				
	.01	.02	.03	.04	.05
3	51	33	28	14	11
5			33	23	15
7				22	23
9					30
\bar{V}	51	33	31	30	20

$$\bar{V} = 33 \text{ km/day}.$$

for $K = 10^{11} \text{ cm}^2 \text{ sec}^{-1}$, diffusion is so rapid that \bar{V} is at least 170 km/day (no table is presented for this last case because a time period of two months did not provide sufficient resolution for accurately computing these speeds). From these data, it appears that a diffusion coefficient of $K = 10^{10} \text{ cm}^2 \text{ sec}^{-1}$ produces isopleth velocities that match the observed meridional speed of propagation of the Martian wave of darkening. Thus, if the meridional propagation of the wave of darkening is a manifestation of a meridional transport of water vapor, a diffusion coefficient equal to $10^{10} \text{ cm}^2 \text{ sec}^{-1}$ is the probable value for the large scale eddy diffusion coefficient in the Martian atmosphere.

4.4 Conclusions

A simple diffusion model to explain the interhemispheric transport of water vapor on Mars has been developed. In the model, it is assumed that initially there is a polar ice cap one centimeter thick extending from 60° latitude to the pole and no initial distribution of water vapor in the atmosphere. At time $t = 0$ this ice cap begins to recede toward the pole at a constant rate and at time $t = 12$ terrestrial months it has completely disappeared. The water vapor released into the atmosphere by the sublimating ice cap is diffused southward by a large scale eddy diffusion process with a constant diffusion coefficient. Computations of latitudinal distributions of water vapor concentration as a function of time with this model suggest that a diffusion coefficient of at least $10^{10} \text{ cm}^2 \text{ sec}^{-1}$ is required to accomplish the interhemispheric transport of water vapor that is necessary to form the south polar cap at the expense of the water originally in the north polar cap. It is also noted that a diffusion coefficient of $K = 10^{10} \text{ cm}^2 \text{ sec}^{-1}$ leads to a meridional velocity of water vapor isopleths equal to 33 km/day, which is in good agreement with the observed meridional speed of propagation of the Martian wave of darkening (30 km/day). On the basis of these computations, it is suggested that large scale eddy diffusion of water vapor from the sublimating polar cap to the forming polar cap can explain the seasonal ice cap cycle on Mars. The required large scale eddy diffusion coefficient is about $10^{10} \text{ cm}^2 \text{ sec}^{-1}$. Such a value is of the same order of magnitude as the large scale eddy diffusion coefficient in the Earth's atmosphere (Bolin and Keeling, 1963).

A more realistic model would include the effect of a sink (forming polar cap) as well as a source (sublimating polar cap) on the water vapor distributions. Development of such a model is planned.

REFERENCES

- Bolin, B., and C.D. Keeling, 1963: Large-scale atmospheric mixing as deduced from the seasonal and meridional variations of carbon dioxide. J. Geophys. Res., 68, 3899-3920.
- De Vaucouleurs, G., 1961: Reconnaissance of the Nearer Planets. Air Force Office of Scientific Research, Tech. Rpt. AFOSR/DRA-51-1, 141 pp.
- Dollfus, A., 1961: Visual and photographic studies of planets at Pic du Midi. Chapter 15 of Planets and Satellites, ed. G.P. Kuiper and B.M. Middlehurst, U. of Chicago Press, 534-571.
- Junge, C., 1962: Global ozone budget and exchange between stratosphere and troposphere. Tellus, 14, 363-377.
- Junge, C., 1963: Studies of global exchange processes in the atmosphere by natural and artificial tracers. J. of Geophys. Res., 68, 3849-3855.
- Kaplan, L.D., G. Munch, and H. Spinrad, 1964: An analysis of the spectrum of Mars. Astrophys. J., 139, 1-15.